

See discussions, stats, and author profiles for this publication at: <https://www.researchgate.net/publication/269988927>

# Novel Tacrine-Grafted Ugi Adducts as Multipotent Anti-Alzheimer Drugs: A Synthetic Renewal in Tacrine-Ferulic Acid Hybrids

ARTICLE *in* CHEMMEDCHEM · DECEMBER 2014

Impact Factor: 2.97 · DOI: 10.1002/cmdc.201402409

CITATIONS

2

READS

133

21 AUTHORS, INCLUDING:



Javier Egea

Instituto de Investigación Sanitaria, Hospit...

72 PUBLICATIONS 916 CITATIONS

SEE PROFILE



Elena Soriano

Spanish National Research Council

92 PUBLICATIONS 1,464 CITATIONS

SEE PROFILE



Maria Laura Bolognesi

University of Bologna

135 PUBLICATIONS 3,153 CITATIONS

SEE PROFILE

# Novel Tacrine-Grafted Ugi Adducts as Multipotent Anti-Alzheimer Drugs: A Synthetic Renewal in Tacrine–Ferulic Acid Hybrids

Mohamed Benchekroun,<sup>[a]</sup> Manuela Bartolini,<sup>[b]</sup> Javier Egea,<sup>[c]</sup> Alejandro Romero,<sup>[d]</sup> Elena Soriano,<sup>[e]</sup> Marc Pudlo,<sup>[a]</sup> Vincent Luzet,<sup>[a]</sup> Vincenza Andrisano,<sup>[f]</sup> María-Luisa Jimeno,<sup>[g]</sup> Manuela G. López,<sup>[c]</sup> Sarah Wehle,<sup>[h]</sup> Tijani Gharbi,<sup>[a]</sup> Bernard Refouvelet,<sup>[a]</sup> Lucía de Andrés,<sup>[i]</sup> Clara Herrera-Arozamena,<sup>[i]</sup> Barbara Monti,<sup>[b]</sup> Maria Laura Bolognesi,<sup>[b]</sup> María Isabel Rodríguez-Franco,<sup>[i]</sup> Michael Decker,<sup>[h]</sup> José Marco-Contelles,<sup>\*,[j]</sup> and Lhassane Ismaili<sup>\*,[a]</sup>

Herein we describe the design, multicomponent synthesis, and biological, molecular modeling and ADMET studies, as well as in vitro PAMPA-blood–brain barrier (BBB) analysis of new tacrine–ferulic acid hybrids (TFAHs). We identified (*E*)-3-(hydroxy-3-methoxyphenyl)-*N*-[8[(7-methoxy-1,2,3,4-tetrahydroacridin-9-yl)amino]octyl]-*N*-[2-(naphthalen-2-ylamino)2-oxoethyl]acrylamide (TFAH **10n**) as a particularly interesting multipotent compound that shows moderate and completely selective inhibition of human butyrylcholinesterase ( $IC_{50}$  = 68.2 nM), strong antioxidant activity (4.29 equiv trolox in an oxygen radical absorbance capacity (ORAC) assay), and good  $\beta$ -amyloid ( $A\beta$ )

anti-aggregation properties (65.6% at 1:1 ratio); moreover, it is able to permeate central nervous system (CNS) tissues, as determined by PAMPA-BBB assay. Notably, even when tested at very high concentrations, TFAH **10n** easily surpasses the other TFAHs in hepatotoxicity profiling (59.4% cell viability at 1000  $\mu$ M), affording good neuroprotection against toxic insults such as  $A\beta_{1-40}$ ,  $A\beta_{1-42}$ ,  $H_2O_2$ , and oligomycin A/rotenone on SH-SY5Y cells, at 1  $\mu$ M. The results reported herein support the development of new multipotent TFAH derivatives as potential drugs for the treatment of Alzheimer's disease.

## Introduction

Alzheimer's disease (AD) is a neurodegenerative disorder characterized by progressive cognitive impairment and memory loss, associated with a deficit in cholinergic neurotransmission.<sup>[1]</sup> Histological changes that underlie this disorder include plaques of  $\beta$ -amyloid ( $A\beta$ ) peptide, neurofibrillary tangles (NFT), a dramatic loss of synapses and neurons, and a de-

creased level of choline acetyltransferase that correlates with a decline in mental status scores.<sup>[2]</sup>

Owing to the multi-pathogenic nature of AD, one of the current drug discovery approaches for AD treatment focuses on compounds with a multitarget biological profile, the so-called multitarget-directed ligands (MTDLs).<sup>[3]</sup> MTDLs developed thus

[a] M. Benchekroun, Dr. M. Pudlo, V. Luzet, Prof. T. Gharbi, Prof. B. Refouvelet, Dr. L. Ismaili  
NanoMedicine, Imagery and Therapeutics Lab EA 4662  
Laboratoire de Chimie Organique et Thérapeutique  
CHRU Jean Minjot, Université de Franche-Comté  
19, rue Ambroise Paré, 25030 Besançon (France)  
E-mail: lhassane.ismaili@univ-fcomte.fr

[b] Dr. M. Bartolini, Prof. B. Monti, Prof. M. L. Bolognesi  
Department of Pharmacy and Biotechnology  
Alma Mater Studiorum, University of Bologna  
Via Belmeloro 6, 40126 Bologna (Italy)

[c] Dr. J. Egea, Dr. M. G. López  
Instituto Teófilo Hernando and  
Departamento de Farmacología y Terapéutica  
Facultad de Medicina, Universidad Autónoma de Madrid  
C/Arzobispo Morcillo 4, 28029 Madrid (Spain)

[d] Dr. A. Romero  
Departamento de Toxicología y Farmacología  
Facultad de Veterinaria  
Universidad Complutense de Madrid, 28040 Madrid (Spain)

[e] Dr. E. Soriano  
SEPCO (IQOG, CSIC), C/Juan de la Cierva 3, 28006 Madrid (Spain)


[f] Prof. V. Andrisano  
Department for Life Quality Studies  
University of Bologna, Corso di Augusto, 237, 47921 Rimini (Italy)

[g] Dr. M.-L. Jimeno  
CENQUIOR (CSIC), C/Juan de la Cierva 3, 28006 Madrid (Spain)

[h] S. Wehle, Prof. Dr. M. Decker  
Pharmazeutische und Medizinische Chemie  
Institut für Pharmazie und Lebensmittelchemie  
Julius-Maximilians-Universität Würzburg  
Würzburg Am Hubland, 97074 Würzburg (Germany)

[i] L. de Andrés, C. Herrera-Arozamena, Prof. M. I. Rodríguez-Franco  
Instituto de Química Médica (IQM-CSIC)  
C/Juan de la Cierva 3, 28006 Madrid (Spain)

[j] Prof. J. Marco-Contelles  
Laboratorio de Química Médica (IQOG, CSIC)  
C/Juan de la Cierva 3, 28006 Madrid (Spain)  
E-mail: iqog21@iqog.csic.es

 Supporting information for this article is available on the WWW under <http://dx.doi.org/10.1002/cmdc.201402409>.

far include derivatives that can simultaneously restore brain acetylcholine (ACh) levels, decrease oxidative stress, inhibit A $\beta$  aggregation, and protect neuronal cells against toxic insults.<sup>[4–6]</sup> Two cholinesterases, acetylcholinesterase (AChE) and butyrylcholinesterase (BuChE), are responsible for hydrolysis of the neurotransmitter ACh in the brain. Recent evidence has highlighted a non-classical role for cholinergic enzymes, which may be important for the development of more effective drugs for AD. Indeed, it was shown that several AChE inhibitors (AChEIs) not only facilitate cholinergic transmission, but also interfere with the synthesis, deposition, and aggregation of toxic A $\beta$ .<sup>[7,8]</sup> Other studies have suggested that BuChE may also influence the aggregation of A $\beta$  into neuritic plaques and formation of the NFT deposit.<sup>[9,10]</sup> Oxidative stress is also thought to play a key role in the pathogenesis of AD. Indeed, many studies have shown that senile plaques release reactive oxygen species (ROS),<sup>[11]</sup> the accumulation of which damages major cell components such as the nucleus, mitochondrial DNA, membranes, and cytoplasmic proteins.<sup>[12]</sup>

Despite the impressive amount of progress in understanding the molecular mechanisms behind AD, an effective drug is still not available; AChEIs such as rivastigmine, galantamine, and donepezil remain the principal class of drugs used in the treatment of this disease.<sup>[13]</sup> Tacrine **1** (Figure 1), a potent, sub-micromolar inhibitor of human AChE (hAChE), was the first FDA-approved drug<sup>[14]</sup> for the treatment of AD. However, it was withdrawn shortly after its 1993 approval<sup>[15]</sup> because of its liver toxicity. In spite of this, studies with tacrine analogues have continued<sup>[16]</sup> in the search for more potent and safer tacrine derivatives. In light of this, it is worth mentioning that the 7-methoxy derivative of tacrine, 9-amino-7-methoxy-1,2,3,4-tetrahydroacridine (7-MEOTA **2**, Figure 1),<sup>[17]</sup> shows lower hepatotoxicity than tacrine.<sup>[18–20]</sup>

Based on the MTDL approach, recent reports have described tacrine hybrids prepared by connecting tacrine or its derivatives to other pharmacologically relevant scaffolds with the aim of overcoming tacrine's hepatotoxicity.<sup>[21]</sup> Among these are the tacrine hybrids, such as the antioxidant tacrine–ferulic acid nitric oxide (NO) donor (hybrid **3**, Figure 1),<sup>[22]</sup> or tacrine–caffeic acid (hybrid **4**, Figure 1).<sup>[23]</sup> Decker and co-workers showed that tacrine–ferulic acid hybrid (TFAH) **5a** (Figure 2) is a moderate antioxidant and a potent reversible noncompetitive AChEI. Hybrid **5a** is able to bind the peripheral anionic site (PAS) of AChE, showing a near equipotent capacity to inhibit *Electrophorus electricus* (Ee) AChE and

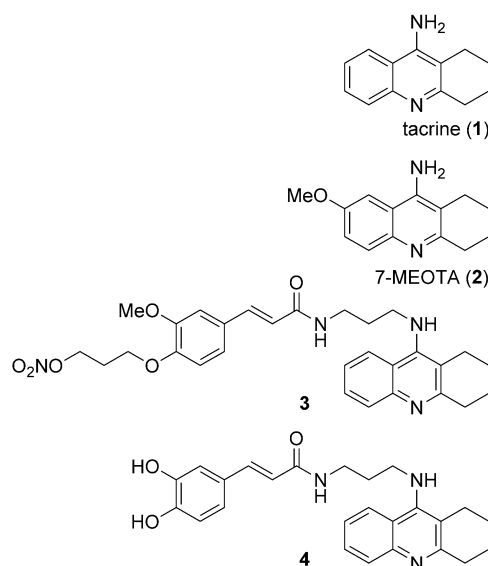


**Figure 1.** Structures of tacrine (**1**), 7-MEOTA (**2**) and tacrine–ferulic acid hybrids **3** and **4**.

equine (eq) BuChE.<sup>[24]</sup> In addition, TFAH **5b** (Figure 2), described by Pi et al.,<sup>[25]</sup> showed significant in vitro inhibition of AChE-induced and self-induced A $\beta_{1–40}$  aggregation, and blocked cell death induced by A $\beta_{1–40}$  in PC12 cells.

From a synthetic point of view, multicomponent reactions have emerged as the method of choice for introducing molecular diversity.<sup>[26]</sup> Therefore, they seem well suited to the search for new molecules with different moieties of interest that are able to interact with various pathological events in connection

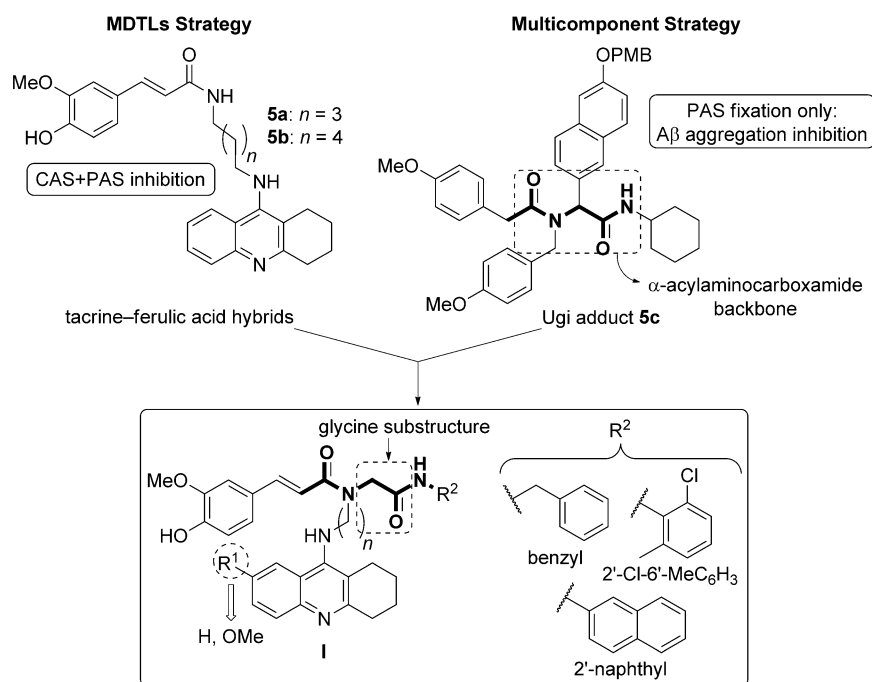


**Figure 2.** Structures of compounds **5a–c**, and the general structure for the new (E)-3-hydroxy-3-methoxyphenyl-N-alkyl-N-[(2-oxo-2-amino)ethyl]acrylamides **I** described in this work.

with AD.<sup>[4,27–29]</sup> Particularly interesting among these types of reactions is the Ugi four-component reaction (U-4CR). This transformation allows the creation of up to five points of structural diversity in one pot which can be very useful for the expeditious synthesis of bioactive molecules for multifactorial diseases such as AD.<sup>[30]</sup>

In this context and by following a docking-driven combinatorial strategy, Dickerson et al. prepared a library of Ugi adducts based on a planar and rigid naphthalene moiety, the so-called “credit-card” compounds.<sup>[31]</sup> As an example, adduct **5c** (Figure 2) is only able to bind the hydrophobic PAS of AChE with its naphthalene moiety, which disrupts the existing hydrophobic interactions between AChE and Aβ, thereby inhibiting AChE-induced Aβ aggregation. The authors also reported that the observed inhibitory activity is not simply elicited by the naphthalene fragment, but is also very likely due to the presence of the substituted α-acylaminocarboxamide backbone.

Considering these precedents and taking advantage of the chemical diversity readily accessible by the U-4CR, herein we report the design, synthesis, and biological evaluation of a new family of TFAHs, namely (*E*)-3-(4-hydroxy-3-methoxyphenyl)-*N*-alkyl-*N*-(2-oxo-2(amino)ethyl)acrylamides (**1**, Figure 2), as part of our efforts to discover new MTDLs for AD therapy. These compounds possess a substituted glycine substructure as part of the main α-acylaminocarboxamide backbone. Consequently, the new adducts contain tacrine or 7-MEOTA motifs, and a feruloyl group, both tethered to the glycine fragment. The carbonyl group of the glycine portion was functionalized as an amide either by benzylamine, 2'-chloro-6'-methylaniline, or 2'-naphthylamine, which should confer additional cholinesterase inhibitory activity and antioxidant properties to the target molecules. We also hypothesized that the substituted glycine substructure in our adducts would afford additional aromatic groups that are able to bind the hydrophobic PAS of AChE, with potential consequences on the aggregation of Aβ.<sup>[32]</sup>

We synthesized 14 new TFAHs, identified as hybrids **10a–n** (Figure 3), and evaluated their hepatotoxicity toward HepG2 cells. We assayed the neuroprotective capacity of some selected hybrids against several toxic insults such as Aβ<sub>1–40</sub>, Aβ<sub>1–42</sub>, H<sub>2</sub>O<sub>2</sub>, and oligomycin A/rotenone, as well as their inhibitory activity toward cholinesterase, Aβ<sub>1–42</sub> self-aggregation, and antioxidant activity (ORAC-FL scavenging test). From these studies, we identified TFAH **10n** [(*E*)-3-(4-hydroxy-3-methoxyphenyl)-*N*-(8-((7-methoxy-1,2,3,4-tetrahydroacridin-9-yl)amino)octyl)-*N*-(2-(naphthalen-2-ylamino)-2-oxoethyl)acrylamide] as new and very promising multipotent hit molecule for further AD drug development.

## Results and Discussion

### Chemistry

The synthesis of the target TFAHs **10a–n** was carried out with the short synthetic procedure depicted in Scheme 1, with good overall yields. 9-Chlorotacrine **8a,b** were synthesized by following known procedures.<sup>[33–35]</sup> The latter chloro compounds

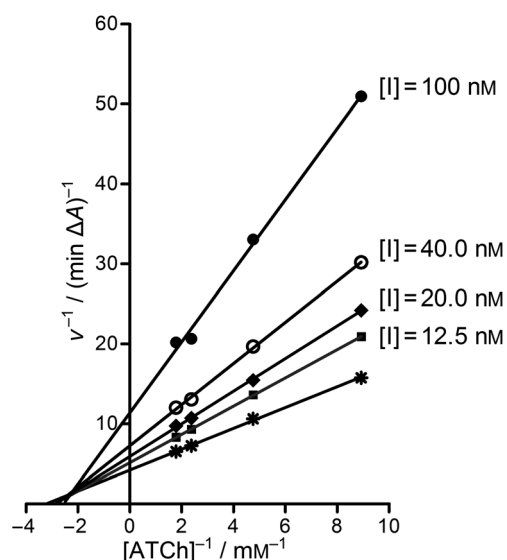
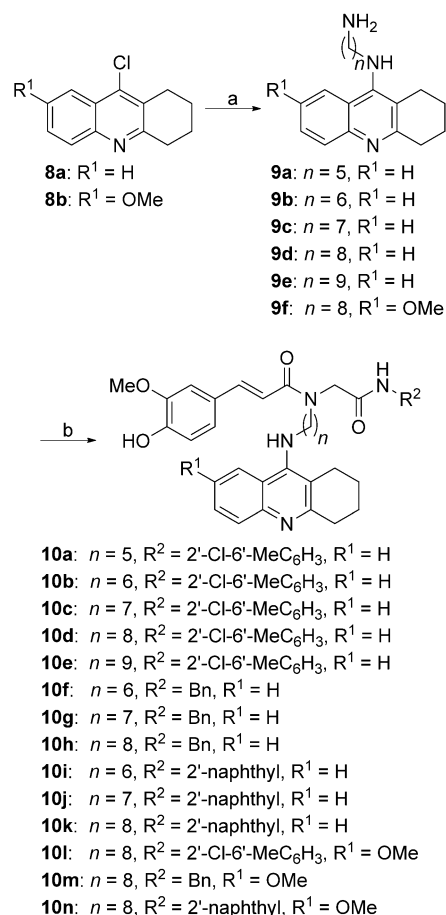


**Figure 3.** Steady-state inhibition of hAChE hydrolysis of acetylthiocholine (ATCh) by TFAH **10h**. Lineweaver–Burk reciprocal plots of initial velocity and substrate concentrations (0.11–0.56 μM) are presented; lines were derived from a weighted least-squares analysis of data.



**Scheme 1.** Synthesis of TFAHs **10a–n**. Reagents and conditions:

a) NH<sub>2</sub>(CH<sub>2</sub>)<sub>n</sub>NH<sub>2</sub> (3.0 equiv), 1-pentanol, reflux, 18 h (54–66%); b) formaldehyde, ferulic acid, isocyanides (benzylisocyanide, 2-chloro-6-methylphenylisocyanide, 2-naphthylisocyanide), MeOH/CH<sub>2</sub>Cl<sub>2</sub> (3:1 v/v), RT, 24 h (16–48%).

were then treated with the appropriate alkylenediamines in 1-pentanol at reflux to obtain diamines **9a–f**. These diamines were then treated, by one-pot U-4CR, with formaldehyde, ferulic acid, and selected commercial isocyanides, in methanol/dichloromethane (3:1 v/v) at room temperature for 24 h to obtain the expected TFAHs **10a–n** in 16–48% overall yields (Scheme 1).<sup>[36]</sup>

All new TFAHs showed analytical and spectroscopic data in good agreement with their structures. Structural characterization of the synthesized (*E*)-3-(4-hydroxy-3-methoxyphenyl)-*N*-alkyl-*N*-[2-oxo-2-(amino)ethyl]acrylamides **10a–n** was carried out by NMR spectroscopy. At 298 K these compounds showed broadened NMR spectra or even multiple NMR signals, indicative of their conformational mobility, which is related to the presence of two or more conformers in solution, as confirmed by an in-depth NMR analysis on selected compounds (variable-temperature <sup>1</sup>H and <sup>13</sup>C NMR, gCOSY, TOCSY, NOESY, ROESY, multiplicity-edited gHSQC and gHMBC; see Supporting Information).

Hybrids **10a–k** bear a tacrine moiety, whereas TFAHs **10l–n** are 7-MEOTA derivatives. As shown in Scheme 1, for tacrine hybrids **10a–k**, R<sup>2</sup> may be either benzyl, 2'-chloro-6'-methylphenyl, or 2'-naphthyl, depending on the commercial isocyanide used for their synthesis, and the length of the linker varies between 5 and 9 methylene units. On the other hand, for hybrids **10l–n**, the linker was kept at *n*=8, while, similar to hybrids **10a–k**, R<sup>2</sup> may be a benzyl, 2'-chloro-6'-methylphenyl, or 2'-naphthyl residue.

## Biological evaluations

The in vitro biological evaluations of the new TFAHs **10a–n** started with investigations of the toxicity profile toward HepG2 cells, and continued with determination of their activity profiles on selected targets, including neuroprotection, inhibition

of cholinesterase activity, antioxidant capacity, and inhibition of Aβ<sub>1–42</sub> self-aggregation.

## Evaluation of hepatotoxicity on HepG2 cells

For the tacrine hybrids **10a–n**, the first and most critical aspect was evaluation of their hepatotoxicity<sup>[37]</sup> across a wide concentration range (1–1000 μM; see Experimental Section). Cell viability was determined by MTT assay carried out with HepG2 cells.<sup>[38]</sup> As expected, tacrine showed dose-dependent cytotoxicity (Table 1), with the inflexion point starting at 100 μM. In general, the hepatotoxic effect of TFAHs **10a–n** after incubation for 24 h was lower than that exerted by tacrine. Concerning the structure–activity relationships (SAR), and based on the observed values at 1000 μM (the highest concentration investigated), several conclusions can be drawn: Not surprisingly, and in agreement with the rationale of their design, hybrids with the 7-MEOTA fragment (**10l–n**) were less toxic than the tacrine hybrids. Only TFAHs **10a** and **10h** showed similar cytotoxicity. The less toxic derivatives at 1000 μM were **10n** and **10m**, bearing both an octamethylene linker and a 2'-naphthyl or benzyl group, respectively, (1.72-fold less toxic than tacrine). The most toxic was compound **10i**, bearing a 2'-naphthyl group as R<sup>2</sup>, and a hexamethylene linker. Among tacrine hybrids **10a–e**, bearing a 2'-chloro-6'-methylphenyl group, the less toxic compound **10a** (1.47-fold less toxic than tacrine at 1000 μM) has a pentamethylene linker, but toxicity increased in going to TFAHs with linkers of *n*=6 and *n*=7, and decreased for compound **10e**, with a nonamethylene linker. A similar trend was also observed in TFAHs **10f–h** bearing a benzyl group as R<sup>2</sup>, with the less toxic **10h** (1.64-fold less than tacrine); for compounds **10i–k** (2'-naphthyl as R<sup>2</sup>), the longer linker, the lower the toxicity.

As a final consideration, the type of substituent at the glycine fragment seems to influence the extent of toxicity toward HepG2 cells. Indeed, very interestingly, comparing the toxicity

**Table 1.** In vitro toxicity of tacrine and TFAHs **10a–n** in HepG2 cells.<sup>[a]</sup>

Compd	1 μM	3 μM	10 μM	30 μM	100 μM	300 μM	1000 μM
<b>10a</b>	99.3 ± 1.7 (ns)	98.9 ± 1.7 (ns)	96.4 ± 1.3 (ns)	66.1 ± 1.1***	62.9 ± 1.3***	57.9 ± 2.5***	50.9 ± 4.1***
<b>10b</b>	99.5 ± 1.3 (ns)	87.4 ± 1.2**	85.9 ± 1.6***	71.4 ± 1.1***	48.7 ± 2.0***	47.5 ± 2.0***	43.2 ± 1.1***
<b>10c</b>	96.1 ± 1.1 (ns)	88.8 ± 1.3 (ns)	85.4 ± 1.8*	82.4 ± 1.5**	50.5 ± 2.6***	46.8 ± 4.1***	43.5 ± 3.1***
<b>10d</b>	98.4 ± 0.7 (ns)	96.3 ± 1.4 (ns)	88.7 ± 1.1*	83.8 ± 1.4***	50.2 ± 2.6***	50.6 ± 2.2***	43.3 ± 1.9***
<b>10e</b>	100.0 ± 1.4 (ns)	97.6 ± 1.6 (ns)	95.6 ± 0.3 (ns)	71.8 ± 1.7***	54.2 ± 1.1***	53.5 ± 0.7***	47.2 ± 2.9***
<b>10f</b>	97.0 ± 1.9 (ns)	92.3 ± 2.1 (ns)	91.8 ± 1.9 (ns)	92.7 ± 1.9 (ns)	63.3 ± 3.7***	50.5 ± 3.8***	48.9 ± 4.4***
<b>10g</b>	85.3 ± 2.4 (ns)	79.0 ± 3.8*	76.0 ± 1.3**	73.1 ± 3.9**	47.2 ± 3.1***	47.0 ± 3.4***	46.3 ± 2.1***
<b>10h</b>	95.2 ± 1.5 (ns)	95.2 ± 1.7 (ns)	94.4 ± 1.7 (ns)	81.2 ± 1.0***	61.8 ± 0.2***	60.1 ± 1.0***	56.3 ± 2.0***
<b>10i</b>	97.1 ± 2.6 (ns)	96.0 ± 0.4 (ns)	94.8 ± 1.6 (ns)	89.7 ± 1.9 (ns)	48.0 ± 2.8***	40.7 ± 2.3***	36.3 ± 1.9***
<b>10j</b>	99.2 ± 1.4 (ns)	95.0 ± 0.8 (ns)	94.5 ± 0.3 (ns)	92.8 ± 1.2 (ns)	63.2 ± 2.9***	44.2 ± 1.3***	39.3 ± 2.0***
<b>10k</b>	97.5 ± 0.3 (ns)	96.1 ± 0.6 (ns)	95.9 ± 1.4 (ns)	91.8 ± 0.9 (ns)	74.6 ± 2.8***	46.8 ± 1.4***	46.1 ± 2.3***
<b>10l</b>	93.5 ± 2.4 (ns)	94.5 ± 1.5 (ns)	88.8 ± 1.6***	56.6 ± 0.9***	51.4 ± 1.7***	52.4 ± 1.4***	50.8 ± 1.0***
<b>10m</b>	100.3 ± 1.1 (ns)	98.9 ± 1.8 (ns)	97.9 ± 2.8 (ns)	98.1 ± 0.9 (ns)	97.0 ± 2.7 (ns)	60.3 ± 2.9***	59.2 ± 1.6***
<b>10n</b>	98.8 ± 2.4 (ns)	97.0 ± 1.8 (ns)	92.0 ± 3.0 (ns)	94.0 ± 3.8 (ns)	83.2 ± 2.5*	74.0 ± 1.4***	59.4 ± 4.7***
tacrine	93.4 ± 4.7 (ns)	90 ± 3.0 (ns)	88.7 ± 3.4 (ns)	81.6 ± 4.9*	64.3 ± 4.5***	40 ± 2.2***	34.4 ± 2.7***

[a] Cell viability was determined by MTT assay. Data are normalized as a percentage of control, and are expressed as the means ± SEM of triplicates from at least three different cultures. All compounds were assayed at increasing concentrations (1–1000 μM, as indicated); \*\*\**p* ≤ 0.001, \*\**p* ≤ 0.01, \**p* ≤ 0.05, and ns: not significant with respect to control group. Comparison between tested hybrids and control group was performed by one-way ANOVA followed by the Newman–Keuls post-hoc test.



of hybrids with the same length linker and different R<sup>2</sup> groups, compounds with a benzyl group [**10 f** (*n* = 6), **10 g** (*n* = 7), **10 h** (*n* = 8)] were found to be consistently less toxic than their analogues with 2'-naphthyl or 2'-chloro-6'-methylphenyl groups.

### Neuroprotective capacity of TFAHs **10 a–n**

The neuroprotective capacity of the five least hepatotoxic compounds **10 a**, **10 e**, **10 h**, **10 m**, and **10 n** were tested for their ability to prevent the human neuroblastoma cell line SH-SY5Y from cell death induced by three toxicity models: 1) Aβ peptides (Aβ<sub>1–40</sub> and Aβ<sub>1–42</sub>), which are implicated in apoptosis-related signaling pathways and ROS production,<sup>[39]</sup> 2) hydrogen peroxide for the generation of exogenous free radicals, and 3) a mixture of oligomycin A and rotenone (O/R), two mitochondrial respiratory chain blockers, which produce mitochondrial ROS by respectively inhibiting complexes V and I of the mitochondrial electron-transport chain. Thus, compounds that are able to block or hamper these toxic insults may be considered neuroprotectants.<sup>[40]</sup> However, prior to the evaluation of neuroprotective capacity, the direct cytotoxicity of the selected TFAHs was investigated at concentrations of 1, 3, and 10 μM. In these experiments, cell viability was measured by MTT assay.<sup>[38]</sup> As shown in Table 2,

Compd	1 μM	3 μM	10 μM
<b>10 a</b>	99.9 ± 6.7 (ns)	100.2 ± 5.5 (ns)	90.8 ± 1.6 (ns)
<b>10 e</b>	94.6 ± 5.2 (ns)	85.5 ± 5.8 (ns)	10.0 ± 3.5***
<b>10 h</b>	91.7 ± 0.6 (ns)	81.6 ± 4.3*	9.9 ± 2.6***
<b>10 m</b>	99.7 ± 1.4 (ns)	79.4 ± 4.7**	40.1 ± 1.9***
<b>10 n</b>	98.9 ± 0.9 (ns)	97.5 ± 1.2 (ns)	95.1 ± 1.4 (ns)

[a] All compounds were assayed for 24 h; \*\*\**p* ≤ 0.001, \*\**p* ≤ 0.01, and ns: not significant with respect to basal levels. Data are expressed as the means ± SEM of triplicates from at least five different cultures.

TFAHs **10 a** and **10 n** were found have no toxicity at all concentrations tested, whereas **10 e**, **10 h**, and **10 m** showed significant toxicity at 3 and 10 μM. Compounds **10 h** and **10 m** remain nontoxic at 1 μM, but exhibited high toxicity at 3 and 10 μM. Consequently, cell-based assays for neuroprotection were carried out at 0.3 and 1 μM for **10 a**, **10 e**, and **10 h**, at 1 μM for **10 m**, and at 1 and 3 μM for **10 n**. TFAH **10 m** showed poor neuroprotection against H<sub>2</sub>O<sub>2</sub> and O/R, but displayed very high and significant neuroprotection against the Aβ<sub>1–42</sub> insult and a moderate effect against Aβ<sub>1–40</sub> (Table 3). Interestingly, at the same concentration, **10 n** displayed opposite, yet quantitatively similar, behavior on Aβ-related cytotoxicity, also showing moderately significant neuroprotection against H<sub>2</sub>O<sub>2</sub> and O/R. However, at 3 μM, the neuroprotection given by compound **10 n** against H<sub>2</sub>O<sub>2</sub> and O/R was drastically decreased; concerning Aβ-induced cytotoxicity, however, the reverse trend

**Table 3.** Protective effect of TFAHs **10 a**, **10 e**, **10 h**, **10 m**, and **10 n** on SH-SY5Y cell death induced by Aβ<sub>1–40</sub>, Aβ<sub>1–42</sub>, H<sub>2</sub>O<sub>2</sub>, or oligomycin A/rotenone.<sup>[a]</sup>

Compd (c [μM])	Aβ <sub>1–40</sub> <sup>[b]</sup>	Aβ <sub>1–42</sub> <sup>[c]</sup>	H <sub>2</sub> O <sub>2</sub> <sup>[d]</sup>	O/R <sup>[e]</sup>
<b>10 a</b> (0.3)	ND	24.7 ± 3.6*	ND	22.3 ± 2.9**
<b>10 a</b> (1)	ND	52.3 ± 4.2***	76.6 ± 1.5***	30.5 ± 1.6**
<b>10 e</b> (0.3)	ND	38.1 ± 2.0**	ND	39.9 ± 1.4***
<b>10 e</b> (1)	ND	57.2 ± 3.9***	57.4 ± 2.8***	30.1 ± 0.7**
<b>10 h</b> (0.3)	ND	16.4 ± 1.7*	ND	37.3 ± 2.0***
<b>10 h</b> (1)	ND	65.4 ± 3.8***	56.8 ± 3.3***	30.6 ± 0.6**
<b>10 m</b> (1)	42.0 ± 1.4*	80.2 ± 4.2***	2.3 ± 3.8 (ns)	15.2 ± 2.3 (ns)
<b>10 n</b> (1)	74.7 ± 1.2***	46.3 ± 4.9*	52.7 ± 6.2*	40.0 ± 2.0*
<b>10 n</b> (3)	49.8 ± 2.4**	59.7 ± 4.2**	19.9 ± 3.6 (ns)	21.9 ± 1.6 (ns)

[a] Data are expressed as percent neuroprotection ± SEM of triplicates from at least four different cultures; \*\*\**p* ≤ 0.001, \*\**p* ≤ 0.01, \**p* ≤ 0.05, and ns: not significant with respect to control; ND: not determined. [b] [Aβ<sub>1–40</sub>] = 30 μM. [c] [Aβ<sub>1–42</sub>] = 30 μM. [d] [H<sub>2</sub>O<sub>2</sub>] = 300 μM. [e] [oligomycin A] = 10 μM, [rotenone] = 30 μM.

was observed: **10 n** is a more effective yet still moderate neuroprotective agent against cytotoxicity induced by Aβ<sub>1–42</sub>. Interestingly, the overall results obtained for TFAHs **10 a**, **10 e**, and **10 h** are better than those of **10 n** at 1 μM. Indeed, the former three compounds demonstrated nearly the same moderate neuroprotection against O/R and significant to higher neuroprotection against H<sub>2</sub>O<sub>2</sub> and cytotoxicity induced by Aβ<sub>1–42</sub>. On the other hand, at 0.3 μM the neuroprotective effect was lower against Aβ<sub>1–42</sub>, but was higher for **10 e** and **10 h** against O/R.

### Inhibition of EeAChE/eqBuChE

In the first exploratory experiments, we used inexpensive and readily available EeAChE and eqBuChE, with tacrine as reference, and the protocol reported by Ellman et al. for the determination of inhibitory potency.<sup>[41]</sup> As listed in Table 4, the less hepatotoxic 7-MEOTA derivatives **10 l–n**, which also show interesting neuroprotective properties, were the least potent cholinesterase inhibitors among all TFAHs investigated. Conversely, TFAHs **10 a–k** were found to be potent BuChEIs, with IC<sub>50</sub> values in the nanomolar range, showing selectivities from 115.5 (TFAH **10 a**) to 1.6 (TFAH **10 b**). The most potent eqBuChEI was TFAH **10 a** (IC<sub>50</sub> = 1.0 ± 0.2 nM, 5.1-fold more potent than tacrine); the most potent EeAChEI was compound **10 c** (IC<sub>50</sub> = 6.2 ± 0.7 nM, 7.2-fold more potent than tacrine).

Regardless of the influence of the linker, TFAHs **10 a–e**, bearing the 2'-chloro-6'-methylphenyl group, were more potent eqBuChEIs than those bearing benzyl (**10 f–h**) or 2'-naphthyl (**10 i–k**) groups. Regarding the influence of linker length on activity, among the **10 a–e** hybrids, the best eqBuChE inhibitory activity was observed for *n* = 5, progressively decreasing from *n* = 6 to *n* = 9, but remaining quite stable around IC<sub>50</sub> values of 2.61 nM. However, for compounds **10 f–h**, the activity progressively increased from *n* = 6 to *n* = 8, and in the **10 i–k** series the order of activity, from the most to less potent, was 8 > 6 > 7. Regarding equipotency for EeAChE and eqBuChE, TFAH **10 c** and **10 d** were found to be the most balanced, showing IC<sub>50</sub> values of ~6.3 and 2.5 nM, respectively. Overall, considering the toxicity and cholinesterase inhibitor data, we conclude that the most balanced compounds are **10 h**, **10 a**, and **10 e**, in this

**Table 4.** Inhibition of EeAChE, eqBuChE, hAChE, and hBuChE by TFAHs **10a–n** and reference compounds.

Compd	<i>n</i>	IC <sub>50</sub> [nM]					
		EeAChE <sup>[a]</sup>	eqBuChE <sup>[a]</sup>	SR <sup>[b]</sup>	hAChE <sup>[d]</sup>	hBuChE <sup>[d]</sup>	SR <sup>[e]</sup>
<b>10a</b>	5	115.5 ± 6.5	1.0 ± 0.2	115.5	52.3 ± 4.3	0.717 ± 0.038	72.9
<b>10b</b>	6	5.4 ± 0.6	3.3 ± 0.3	1.6	102 ± 6	0.968 ± 0.055	105.4
<b>10c</b>	7	6.2 ± 0.7	2.6 ± 0.3	2.4	70.0 ± 4.1	0.307 ± 0.020	228
<b>10d</b>	8	6.5 ± 0.1	2.4 ± 0.1	2.7	42.5 ± 2.9	0.336 ± 0.028	126.5
<b>10e</b>	9	26.8 ± 1.9	3.0 ± 0.3	9.0	14.3 ± 1.1	0.318 ± 0.024	45.0
<b>10f</b>	6	14.6 ± 2.1	6.0 ± 1.9	2.4	169 ± 10	2.51 ± 0.17	67.3
<b>10g</b>	7	14.1 ± 0.9	2.8 ± 0.1	5.0	71.0 ± 4.3	1.06 ± 0.07	67.0
<b>10h</b>	8	7.6 ± 0.4	2.8 ± 0.1	2.7	40.1 ± 2.8	0.98 ± 0.09	40.9
<b>10i</b>	6	48.4 ± 0.4	9.1 ± 1.3	5.3	174 ± 15	2.48 ± 0.21	70.2
<b>10j</b>	7	25.3 ± 4.8	11.7 ± 2.2	2.2	65.0 ± 3.3	0.737 ± 0.071	88.2
<b>10k</b>	8	14.9 ± 1	5.9 ± 0.3	2.5	76.5 ± 6.8	0.260 ± 0.021	294.2
<b>10l</b>	8	134.3 ± 8.1	88.9 ± 5.7	1.5	2119 ± 136	14.8 ± 1.1	143.2
<b>10m</b>	8	110.0 ± 8.4	48.8 ± 2.3	2.3	1326 ± 43	49.0 ± 2.6	27.1
<b>10n</b>	8	51.9 ± 3.5 <sup>[c]</sup>	70.5 ± 1.8 <sup>[c]</sup>	–	22.2 ± 1.6 <sup>[c]</sup>	68.2 ± 3.9	–
7-MEOTA	–	ND	ND	–	13 500 ± 900	6400 ± 420	2.1
tacrine	–	44.3 ± 1.5	5.1 ± 0.2	8.7	424 ± 21	45.8 ± 3.0	9.3
FA	–	ND	ND	–	NA	NA	–

[a] Inhibition curves were obtained by nonlinear regression; Ee: electric eel, eq: equine. Data are the mean ± SEM of quadruplicates from at least three different experiments. [b] Selectivity ratio: IC<sub>50</sub>(EeAChE)/IC<sub>50</sub>(eqBuChE). [c] Percent inhibition at 3 μM. [d] Human recombinant AChE and human serum BuChE were used; data are the mean ± SEM of at least three different experiments. [e] Selectivity ratio: IC<sub>50</sub>(hAChE)/IC<sub>50</sub>(hBuChE). ND: not determined; NA: not active at the highest concentration tested (0.2 mM).

order, as they are 1.5-, 1.45- and 1.34-fold less toxic than tacrine at 300 μM, with high eqBuChE activity, and from potent to moderate EeAChE inhibitory activities. Results from these experiments with eel and equine cholinesterases confirm the feasibility of our initial plan regarding the use of a tacrine-grafted α-acylaminocarboxamide backbone in the new TFAHs **10a–k**, in terms of synthetic access and cholinesterase inhibition profiles. This allowed us to proceed with the next step, which was to analyze the capacity of these TFAHs to inhibit human cholinesterases.

#### Inhibition of human AChE/human BuChE and kinetic inhibition studies

As shown in Table 4, and in agreement with data obtained on EeAChE, the less toxic 7-MEOTA derivatives **10l–n** were the less potent hChEIs but better than 7-MEOTA itself (**2**, Figure 1). TFAHs **10a–k** were potent hAChE inhibitors with IC<sub>50</sub> values in the nanomolar range and very potent hBuChE inhibitors, with selectivities ranging from 292.3 (hybrid **10k**) to 40.9 (hybrid **10h**). Relative to eqBuChE inhibition data, IC<sub>50</sub> values for the inhibition of hBuChE were much lower for the same compound for any of the **10a–e** (0.307–0.968 nM), **10f–h** (0.98–2.51 nM), or **10i–k** (0.260–2.48 nM) series. The most potent hBuChEI was TFAH **10k** (IC<sub>50</sub> = 0.260 ± 0.021 nM, 176.1-fold more potent than tacrine). For the same length of linker, TFAHs **10a–e**, bearing the 2'-chloro-6'-methylphenyl group, were more potent hBuChEIs than those bearing benzyl (**10f–h**) or 2'-naphthyl (**10i,j**) groups, except **10k**. Regarding the influence of the linker on activity, in TFAHs **10f–h** and **10i–k** hybrids, hBuChE inhibition decreased in going from *n* = 6 to *n* = 8. For TFAHs **10a–e**, the best was found for *n* = 7 but remain-

ing quite stable in IC<sub>50</sub> values, ~0.32 nM, in going from *n* = 7 to *n* = 9. Concerning inhibition of hAChE, the most potent was compound **10e** (IC<sub>50</sub> = 14.3 ± 1.1 nM, 29.6-fold more potent than tacrine). The following influence of the linker on activity was observed: IC<sub>50</sub> values decreased in going from *n* = 6 to *n* = 9 for TFAHs **10b–e** and from *n* = 6 to *n* = 8 for TFAHs **10f–h** and **10i–k**. Regarding equipotency between hAChE and hBuChE, TFAH **10e** was found to be the most balanced, showing respective IC<sub>50</sub> values of 14.3 and 0.318 nM for hAChE and hBuChE. However, TFAH **10h** is the most balanced of the multipotent hybrids, less toxic than tacrine, and is able to strongly inhibit human AChE and BuChE.

The mechanism of hAChE inhibition by TFAH **10h** was investigated by double-reciprocal Lineweaver–Burk plots, which showed increasing slopes and increasing intercepts with higher inhibitor concentrations. The interception of the lines above the x-axis (Figure 3) indicates that hybrid **10h** is able to interact with both the free and acylated enzyme, and behaves as a mixed-type inhibitor of hAChE. The inhibitor dissociation constants *K<sub>i</sub>* (dissociation constant for the enzyme–inhibitor complex) and *K'<sub>i</sub>* (dissociation constant for the enzyme–inhibitor–substrate complex) were estimated to be 44.1 and 57.2 nM, respectively. Encouraged by these results, and to investigate the multipotency of the new TFAHs, the antioxidant activity and the ability to inhibit Aβ<sub>1–42</sub> self-aggregation were evaluated.

#### Antioxidant activity

The ability of hybrids **10a–n** to decrease the amount of peroxyl radicals was determined by the oxygen radical absorbance capacity by fluorescence (ORAC-FL) method,<sup>[42,43]</sup> using fluorescein (FL) as the fluorescent probe and trolox (6-hydroxy-2,5,7,8-tetramethylchroman-2-carboxylic acid) as standard compound. Results are expressed as trolox equivalents (μmol trolox per μmol test compound). Ferulic acid was also tested, giving an ORAC value of 3.7, in full agreement with the value previously described.<sup>[24]</sup> As shown in Table 5, all TFAH derivatives were able to reduce the amount of peroxyl radical; ORAC values ranged between 3.43 (TFAH **10i**) and 7.74 (TFAH **10b**), similarly to ferulic acid (3.7). TFAHs **10i–k**, bearing the 2'-naphthyl group, were the less potent with nearly the same value. Concerning the 7-MEOTA derivatives (**10l–n**) with the same linker length, compound **10m**, bearing a benzyl group, showed higher activity than TFAHs **10l** and **10n**.

**Table 5.** ORAC values and inhibition of self-induced A $\beta_{1-42}$  aggregation by TFAHs **10a–n** and reference compounds.

Compd	ORAC <sup>[a]</sup>	Inhibition [%] <sup>[b]</sup>
<b>10a</b>	6.89 $\pm$ 0.08	73.5 $\pm$ 0.2
<b>10b</b>	7.74 $\pm$ 0.26	50.1 $\pm$ 2.8
<b>10c</b>	6.40 $\pm$ 0.47	75.0 $\pm$ 1.1
<b>10d</b>	5.29 $\pm$ 0.16	76.7 $\pm$ 0.8
<b>10e</b>	4.41 $\pm$ 0.04	80.8 $\pm$ 1.5
<b>10f</b>	5.75 $\pm$ 0.32	67.9 $\pm$ 4.2
<b>10g</b>	7.04 $\pm$ 0.24	75.0 $\pm$ 1.2
<b>10h</b>	6.40 $\pm$ 0.47	69.3 $\pm$ 3.5
<b>10i</b>	3.43 $\pm$ 0.16	72.0 $\pm$ 0.3
<b>10j</b>	3.57 $\pm$ 0.11	69.0 $\pm$ 1.5
<b>10k</b>	3.44 $\pm$ 0.09	73.0 $\pm$ 1.5
<b>10l</b>	4.79 $\pm$ 0.39	72.4 $\pm$ 1.3
<b>10m</b>	6.47 $\pm$ 0.10	72.1 $\pm$ 3.2
<b>10n</b>	4.29 $\pm$ 0.19	65.6 $\pm$ 0.9
7-MEOTA	ND	< 5 %
tacrine	0.2 $\pm$ 0.1 <sup>[24]</sup>	< 5 %
FA	3.7 $\pm$ 0.1	ND

[a] Data are expressed as  $\mu\text{mol trolox}$  per  $\mu\text{mol}$  test compound and are the mean  $\pm$  SD of  $n=3$  experiments performed in triplicate; ND: not determined. [b] A $\beta_{1-42}$  self-aggregation: [A $\beta_{1-42}$ ] = 50  $\mu\text{M}$ , [inhibitor] = 50  $\mu\text{M}$ .

### Inhibition of A $\beta_{1-42}$ self-aggregation

The inhibitory activity of hybrids **10a–n** against the spontaneous aggregation of A $\beta_{1-42}$  was determined *in vitro* by using a thioflavin T (ThT)-based fluorimetric assay.<sup>[44]</sup> Interestingly, all TFAHs showed A $\beta_{1-42}$  anti-aggregation activity (Table 5), with percent inhibition values in the range 50.1–80.8% when tested at equimolar concentrations with A $\beta_{1-42}$  ([inhibitor] = [A $\beta_{1-42}$ ] = 50  $\mu\text{M}$ ). These data further confirm that these compounds are able to directly inhibit the formation of toxic A $\beta$  species, as previously observed in cell based-assays (Table 3). Notably, reference compounds tacrine and 7-MEOTA were unable to significantly interfere with amyloid aggregation. The most potent A $\beta_{1-42}$  anti-aggregation agent was TFAH **10e** (80.8%), but 7-MEOTA derivatives **10l** and **10m** also showed excellent values of ~72%, yet no clear SAR could be drawn.

### Molecular modeling

TFAH **10b** (Supporting Information), TFAH **10e** (the most active compound against hAChE and the most potent A $\beta_{1-42}$  anti-aggregating agent), and TFAH **10h** (the most active of the **10f–h** series, being the most balanced multipotent antioxidant hybrid, less toxic than tacrine, and able to strongly inhibit hAChE and hBuChE) were used for docking with hAChE (PDB ID: 4EY7)<sup>[45]</sup> and hBuChE (PDB ID: 4BDS).<sup>[46]</sup> Notably, the flexibility and size of these ligands provided several solutions, although a thorough inspection of the binding modes and energy values led to the putative binding modes discussed below.

The modeling results suggest that TFAHs **10e** and **10h** are bound into the catalytic triad (Ser203, His447, and Glu334) of hAChE, oriented along the active site gorge, extending from the catalytic site at the bottom of the gorge to the PAS near the mouth of the gorge, via hydrophobic interactions with var-

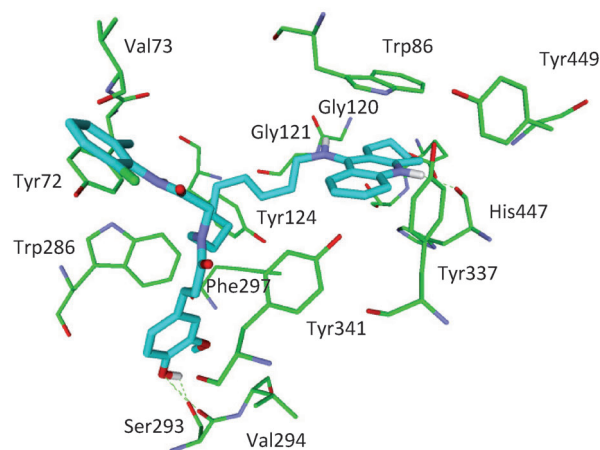


**Figure 4.** Representation of the binding mode of compound TFAH **10e**, shown as cyan sticks, with hAChE (PDB ID: 4EY7). The key residues that interact with the molecule are depicted as thin sticks in green.

ious aromatic residues (Figure 4). Specifically, the predicted binding mode indicates that the tricyclic tetrahydroacridine moiety is engaged in the formation of a characteristic cation– $\pi$  interaction with Trp86 (the choline binding site) and T-shaped stacking interactions with Tyr337. The protonated form of tacrine unit undergoes a hydrogen bond with the carbonyl group of His440. Steric clashes with the methoxy substituent at the tacrine unit in compounds **10l–n** with the hydrophobic pocket formed by Tyr341 and Tyr337 could explain the decrease in inhibitory activity.<sup>[47]</sup> At the mouth of the gorge, the ring of the 2'-chloro-6'-methylphenyl group (or the benzyl group in TFAH **10h**) is  $\pi$ -stacked with Tyr72, a key residue in PAS. The presence of the electron-withdrawing chloro substituent (TFAH **10e**) on the aromatic pendant could lead to reinforcement of the  $\pi$ – $\pi$  interaction, which also seems more effective due to a shorter R<sup>2</sup> substituent (than those bearing the benzyl moiety, as in TFAH **10h**).

In addition, the feruloyl moiety of the  $\alpha$ -acylaminocarboxamide backbone is hydrogen bonded with Ser293 and interacts at PAS with the aromatic core of Trp286 in this predicted binding mode. It has been estimated that the PAS site is ~20 Å away from the CAS.<sup>[48]</sup> The extended conformations of TFAHs **10e** and **10h** have respective lengths of 21.2 and 20.8 Å from the tacrine unit wing to the end of the ferulic acid moiety, which is sufficient to cover both the PAS and CAS, leading our compounds to act as dual binding site inhibitors. Finally, the linker fills a hydrophobic pocket delineated by the phenyl rings of Tyr121, Phe297, and Tyr341, while the amine group is engaged in polar contacts with Gly120 and Gly121.

The inhibitor TFAH **10e** was additionally docked by a method previously reported by Darras et al.,<sup>[49]</sup> which takes seven structural water molecules of AChE into account (Figure 5). In this way, the consistency of the binding mode throughout different docking programs could be explored. This led to the finding of a theoretical binding mode that can explain the interaction with both CAS and PAS. The presented pose of TFAH **10e** shows the tacrine moiety located in the CAS. The tacrine can be stabilized by a 2.8-Å-long hydrogen



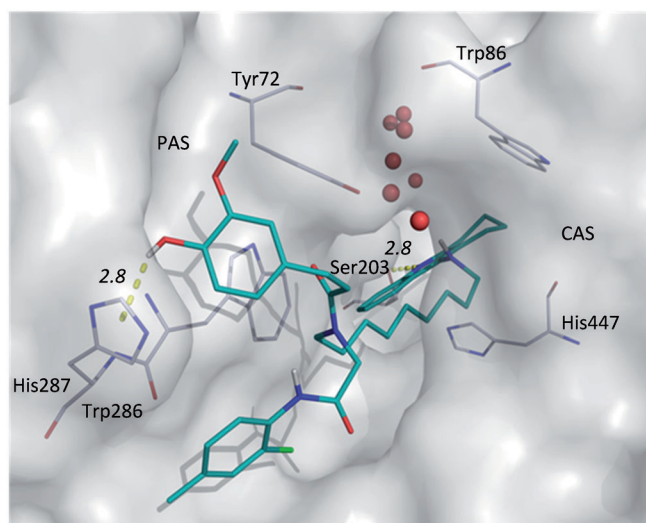


**Figure 5.** Representation of the binding mode of TFAH **10e** (blue) in hAChE (PDB ID: 4EY7, surface representation in gray) with seven structural water molecules (red) obtained by the GOLD software package. Distances (Å) are indicated in italic numerals and were measured in PyMOL.<sup>[50]</sup>

bond to Ser203. The alkyl linker spans the binding gorge, and the amide residues, including feruloyl, are located at the PAS of AChE (Figure 5). At the entrance of the binding pocket the feruloyl can be stabilized by the formation of a hydrogen- $\pi$  interaction of 2.8 Å with the  $\pi$ -electron system of His287. As it becomes visible in the surface representation of AChE, the feruloyl portion of the  $\alpha$ -acetylamino-carboxamide backbone fits perfectly into the groove at the entrance of the binding site, thus inhibiting the PAS of AChE. This is first due to the presence of water molecules, which force the tacrine into a different orientation from the pose without water. Furthermore, the linker adopts a more linear orientation in the docking pose with water. Lastly, in both presented poses, at least one of the aromatic rings supported by the  $\alpha$ -acetylamino-carboxamide chain blocks the PAS. To predict the presence of structural water molecules is not straightforward; therefore, two possible modes of action—with structural water molecules and without—are presented.

The predictive binding mode for the interaction of the ligand TFAH **10e** with the target structure hBuChE is depicted in Figure 6. The tacrine unit of the ligand is  $\pi$ - $\pi$  stacked against the aromatic rings of Trp82 and His438, and its protonated pyridine nitrogen atom is hydrogen bonded to the carbonyl group of His438. Other hydrophobic interactions are formed with Trp430, Tyr440, Met437, and Gly439. This disposition in the active site is the same as that adopted by the tacrine ligand in the enzyme according to crystallographic data.

The hydrophobic 2'-chloro-6'-methylphenyl moiety was observed to fit well within a hydrophobic pocket composed of Pro285, Thr284, Ala328, and Gly283. Moreover, the methoxyphenol group is  $\pi$ -stacked (T-shaped) against the aromatic ring of Phe329, while the hydroxy group and the methoxy substituent are hydrogen bonded to the Ser198 side chain and the Gly117 main chain, respectively. This substituent also forms CH- $\pi$  interactions with Trp231 and other hydrophobic interac-

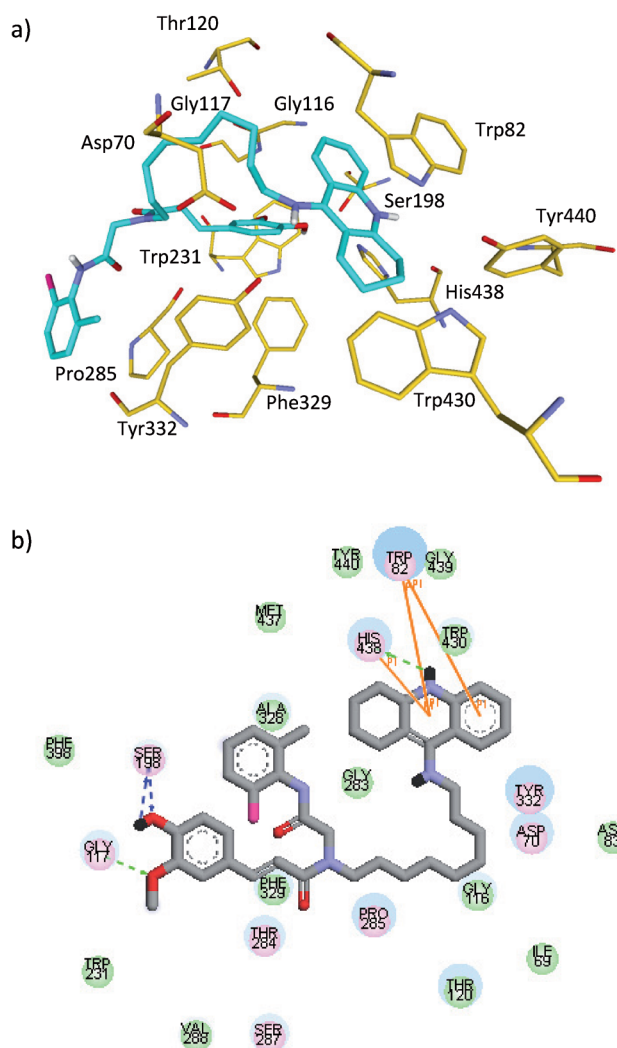


**Figure 6.** a) Representation of the binding mode of TFAH compound **10e**, shown as a cyan stick model, with hBuChE (PDB ID: 4BDS). The key residues that interact with the molecule are depicted as thin sticks in orange. b) 2D diagram of the ligand-protein interactions (hydrogen bond donors and acceptors are represented with blue and green dashed lines, respectively).

tions with Phe398 and Val288. Polar interactions are also observed with Thr284, Pro285, and Ser287.

The tether link is fitted through hydrophobic and polar interactions with Ile69, Asn83, Gly116 and Thr120, and Asp70 and Tyr332, respectively (Figure 6). For TFAH **10h**, a similar binding mode is observed from docking simulations. However, the high degree of flexibility of these ligands permits stacking interactions that involve a different aromatic ring. Thus, the lowest binding energy for TFAH **10h** implies stacking interactions of the benzyl moiety with Phe329, as with the methoxyphenol group of TFAH **10e**, while this one forms  $\sigma$ - $\pi$  interactions with Ser287 and hydrogen bonds, via oxygenated substituents, with Asn289.

### In silico ADMET analysis

Various well-known AChEIs such as ensaculine, donepezil, propidium, rivastigmine, and tacrine have shown to yield modest

improvements in cognitive and memory disorders. However, nitrogen-containing AChEIs have certain side effects and lower central nervous system (CNS) permeability. Thus, new drugs for AD treatment should have a suitable CNS penetration profile and minimal side effects. Indeed, one of the most important requirements for a successful CNS drug is to penetrate and reach its therapeutic targets.

To evaluate this aspect, key parameters related to ADMET properties,<sup>[51–53]</sup> with special emphasis on the requirements of the CNS, were calculated (Table 2S, Supporting Information). The calculated lipophilicity (expressed as  $\log P$ ) and molecular weight ( $M_r$ ) for this series violate Lipinski's rules for both parameters ( $\log P < 5$ ,  $M_r > 500$  Da).<sup>[54]</sup> CNS drugs require more strict rules for successful penetration into their target tissues. Thus, the optimal physicochemical properties for a compound targeting the CNS<sup>[55]</sup> were rationalized as having a  $\log P$  value of 2.8,  $M_r = 305$  Da, a topological polar surface area (TPSA) of 44.8 Å<sup>2</sup>, and a hydrogen bond donor count of 1. For the series under study, the predicted values fall out the appropriate ranges.

Our estimates of blood–brain barrier (BBB) penetration suggested a moderate absorption into CNS tissues for all hybrids, but low absorption for TFAHs **10e**, **10l**, and **10n**. In this sense, observations made by a research team at Pfizer suggested that CNS penetration decreases with increasing  $M_r$ .<sup>[56]</sup> In addition, TFAHs **10l** and **10n** present high TPSA values. According to the computed values of brain penetration,<sup>[57]</sup> TFAHs **10a**, **10b**, **10c**, and **10f** should be the best candidates of the series to act as CNS-active compounds.

Another important parameter to be considered for an oral drug is intestinal permeability. On the basis of the models applied, all the structures show adequate intestinal ( $P_e$ ) and apparent Madin–Darby canine kidney (MDCK) permeability to be good candidates ( $P_e > 0.1$ , MDCK > 25), and should be well absorbed (%HIA). Furthermore, a mid-range level of Caco-2 cell permeability is predicted.<sup>[58]</sup>

Finally, plasma protein binding is a parameter that affects drug availability to the target receptor or enzyme. Indeed, the less bound a drug is, the more efficiently it can traverse cell membranes or diffuse to reach the site of action. The percent of drug bound with plasma proteins was estimated, and compounds were predicted to bind to plasma proteins only weakly; therefore, they are expected to be available for diffusion or transport across cell membranes, thereby interacting with their targets. As previously observed,<sup>[56]</sup> plasma protein binding increased with molecular weight.

Regarding toxicity issues in the drug development phase, early evaluation of a drug's potential to block human ether-à-go-go related gene (hERG) channels is suggested to avoid significant side-effect liabilities, such as QT interval prolongation, in downstream clinical trials. According to the results of our predictions, all hybrids show hERG liability.<sup>[59]</sup> However, none of the hybrids are predicted to induce carcinogenicity in chronic mouse studies. In addition, the models suggest that all compounds, except TFAHs **10m** and

**10n**, present hepatotoxicity.<sup>[60]</sup> In summary, the structures were predicted to have moderate to low brain-penetration profiles, with hybrids **10a**, **10b**, **10c**, and **10f** having the best predicted BBB penetration among the TFAHs synthesized in this study. To confirm the virtual BBB predictions, next we carried out in vitro BBB permeation assays with some selected TFAHs.

### In vitro BBB permeation assays

Many methods have been developed to determine the blood–brain barrier permeation of compounds under investigation. Among them, parallel artificial membrane permeation assays (PAMPA) have the advantage of successfully predicting passive BBB permeation with high throughput and reproducibility. In this assay, the brain penetration of TFAHs **10a–n** was predicted with the in vitro PAMPA-BBB assay described by Di et al.,<sup>[61]</sup> as partially modified by Rodríguez-Franco et al. for assaying molecules with limited water solubility.<sup>[62,63]</sup> The permeability of hybrids ( $P_e$ ) through a lipid extract of porcine brain was determined over the course of 2 h at room temperature by using phosphate-buffered saline (PBS)/ethanol (70:30 v/v) as solvent; the results are listed in Table 6. In the same assay, 11 commercial drugs of known CNS penetration were also tested, and their values were compared with reported values, giving a good linear correlation:  $P_{e, \text{exptl}} = (1.48 P_{e, \text{lit.}}) + 7.14$  ( $R^2 = 0.93$ ). From this equation and following the pattern established by Di et al. for BBB permeation prediction,<sup>[61]</sup> we can predict compounds as follows: CNS + (high BBB permeation) if  $P_e > 13.0 \times 10^{-6} \text{ cm s}^{-1}$ ; CNS – (low BBB permeation) if  $P_e < 10.0 \times 10^{-6} \text{ cm s}^{-1}$ ; and CNS +/- (uncertain BBB permeation) if  $P_e$  ( $10^{-6} \text{ cm s}^{-1}$ ) is between these values (Table 6). The best results for the CNS permeation were obtained for the 7-MEOTA derivatives, **10m** and **10n**, respectively bearing benzyl and naphthyl groups. Interestingly, the best predicted BBB penetration TFAHs **10a**, **10b**, **10c**, and **10f** showed no permeability in this assay. In the case of TFAH **10a**, and not surprisingly, brain penetration, assessed through an ex vivo determination of its AChE inhibitory activity (see Experimental Section below), was not observed.<sup>[64]</sup>

**Table 6.** Permeability values from the PAMPA-BBB assay of TFAHs **10a–n**.<sup>[a]</sup>

Compd	<i>n</i>	<i>R</i> <sup>2</sup>	<i>R</i> <sup>5</sup>	PAMPA-BBB	
				<i>P<sub>e</sub></i> [ $10^{-6} \text{ cm s}^{-1}$ ]	Prediction
<b>10a</b>	5	2'-Cl-6'-MeC <sub>6</sub> H <sub>3</sub>	H	6.5 ± 0.3	CNS –
<b>10b</b>	6	2'-Cl-6'-MeC <sub>6</sub> H <sub>3</sub>	H	6.1 ± 0.2	CNS –
<b>10c</b>	7	2'-Cl-6'-MeC <sub>6</sub> H <sub>3</sub>	H	7.6 ± 0.3	CNS –
<b>10d</b>	8	2'-Cl-6'-MeC <sub>6</sub> H <sub>3</sub>	H	11.0 ± 0.4	CNS +/-
<b>10e</b>	9	2'-Cl-6'-MeC <sub>6</sub> H <sub>3</sub>	H	16.1 ± 0.8	CNS +
<b>10f</b>	6	Bn	H	6.6 ± 0.6	CNS –
<b>10g</b>	7	Bn	H	7.2 ± 0.5	CNS –
<b>10k</b>	8	2'-naphthyl	H	27.6 ± 1.4	CNS +
<b>10m</b>	8	Bn	OMe	13.2 ± 0.4	CNS +
<b>10n</b>	8	2'-naphthyl	OMe	61.5 ± 4.5	CNS +

[a] Results are the mean ± SD of three independent experiments.

## Conclusions

From all the biological and physicochemical results gathered in this study, we have identified TFAH (*E*)-3-(4-hydroxy-3-methoxyphenyl)-*N*-(8-((7-methoxy-1,2,3,4-tetrahydroacridin-9-yl)amino)octyl)-*N*-(2-(naphthalen-2-ylamino)-2-oxoethyl)acrylamide (**10n**) as suitable multipotent TFAH for further development. TFAH **10n** shows moderate and selective hBuChE inhibition ( $IC_{50} = 68.2 \pm 3.9$  nM), ability to penetrate into the CNS, strong antioxidant activity (4.29, ORAC test), inhibition of  $A\beta_{1-42}$  self-aggregation (65.6%), and easily surpasses the other TFAHs in the hepatotoxicity profile (59.4%, 1.72-fold less toxic than tacrine, at 1000  $\mu$ M), affording good neuroprotection against toxic insults such as  $A\beta_{1-40}$ ,  $A\beta_{1-42}$ ,  $H_2O_2$ , and oligomycin A/rotenone, on SH-SY5Y cells, at 1  $\mu$ M. The potency and selectivity of these TFAHs against BuChE is notable, as it is very well known that AChE levels are decreased and BuChE activity is elevated in patients with moderate to severe forms of AD,<sup>[65]</sup> suggesting that ACh hydrolysis in cholinergic synapses may largely occur via BuChE catalysis.<sup>[66]</sup> This suggests that specific inhibition of BuChE may be important in raising ACh levels and improving cognition in patients with moderate forms of AD.<sup>[67]</sup>

We believe the results reported herein support the development of new TFAH derivatives as valuable multipotent drugs for the treatment and prevention of AD. We have also demonstrated and validated the use of the Ugi four-component reaction for the discovery of new MTDLs for AD therapy. This study provides the basis for the future design of entirely new MTDL libraries with up to five pharmacologically relevant scaffolds in one step via the U-4CR or its many variations.

## Experimental Section

**General methods for synthesis:** All reagents were of analytical grade and were used without further purification. All reactions were monitored by TLC using pre-coated silica gel aluminum plates (Macherey–Nagel) and visualized by UV light. Flash column chromatography was carried out with silica gel 60 (70–230 mesh, Macherey–Nagel).  $^1H$  and  $^{13}C$  NMR (JMOD sequence) spectra were acquired at 300 and 75 MHz, respectively, on a Bruker AC300 spectrometer (Bruker BioSpin). Chemical shifts ( $\delta$ ) are reported in parts per million (ppm) relative to the residual solvent signals, and coupling constants ( $J$ ) are reported in hertz (Hz). The following abbreviations are used: s, singlet; bs, broad singlet; d, doublet; dd, doublet of doublet; t, triplet; q, quadruplet; quintuplet, quint; m, multiplet. IR spectra were recorded on a PerkinElmer Spectrum 65 spectrophotometer using an attenuated total reflectance (ATR) device ( $\bar{\nu}$  in  $cm^{-1}$ ). High-resolution MS data were obtained at the Centre Commun de Spectrométrie de Masse, Lyon (France) on a Bruker micrOTOF-Q II spectrometer (Bruker Daltonics) in positive electrospray ionization-time of flight (ESI-TOF) mode. The TFAHs were found to be  $\geq 95\%$  pure by HPLC analysis using a Hitachi Lachrom Elite series instrument equipped with a L2400 Lachrom Elite DAD detector and a Uptisphere ODB column (4.6 mm  $\times$  100 mm,  $\phi = 3$   $\mu$ m). Peaks were detected at  $\lambda$  210 nm, and the system was operated at 25 °C at a flow rate of 2 mL min<sup>-1</sup>. The mobile phase was an isocratic mixture of  $CH_3CN$  and  $H_2O$  (1:1 v/v) containing 0.1% (w/v) monopotassium phosphate.

**General procedure for the synthesis of compounds 9a–f:** 9-Chlorotacrine (**9a–f**, 1.0 mmol, 1 equiv), alkylendiamine (3.0 mmol, 3 equiv), and pentan-1-ol (3 mL) were combined and heated at reflux for 18 h. The reaction was cooled to room temperature, diluted with  $CH_2Cl_2$  (50 mL), and washed with a 10% (w/v) aqueous KOH solution (2  $\times$  50 mL) and  $H_2O$  (2  $\times$  50 mL). The organic layer was dried over  $Na_2SO_4$  and concentrated under reduced pressure to afford the crude product, which was purified by flash column chromatography,  $CH_2Cl_2$ /MeOH/aqueous 30%  $NH_3$  (7:3:0.1 v/v), to afford products **9a–f**. Analytical data of the tacrine linkers **9a–f** are in good agreement with previously described data.<sup>[33]</sup>

**General procedure for the synthesis of TFAHs 10a–n:** A solution of the corresponding *N*'-(1,2,3,4-tetrahydroacridin-9-yl)alkane-1,*n*-diamine **9a–e** or *N*'-(7-methoxy-1,2,3,4-tetrahydroacridin-9-yl)alkane-1,8-diamine **9f** (1.0 mmol) and paraformaldehyde (1.0 mmol) in MeOH/ $CH_2Cl_2$  (7 mL, 3:1 v/v) was stirred for 1 h at room temperature. Ferulic acid (1.0 mmol) and the corresponding isocyanide (1.0 mmol) were then added, and the reaction was stirred for 24 h at room temperature. The mixture was subsequently concentrated under reduced pressure to dryness, and the crude product was purified by flash column chromatography to afford the corresponding TFAHs. Note regarding the  $^1H$  and  $^{13}C$  spectra of TFAHs **10a–n**: At 298 K, some Ugi adducts may appear as a mixture of conformers.

**(*E*)-*N*-(2-((2-Chloro-6-methylphenyl)amino)-2-oxoethyl)-3-(4-hydroxy-3-methoxyphenyl)-*N*-(5-((1,2,3,4-tetrahydroacridin-9-yl)amino)pentyl)acrylamide (**10a**):** *N*'-(1,2,3,4-tetrahydroacridin-9-yl)pentane-1,5-diamine (**9a**) (215 mg, 0.76 mmol), paraformaldehyde (22 mg, 0.76 mmol), ferulic acid (147 mg, 0.76 mmol), and 2-chloro-6-methylphenylisocyanide (115 mg, 0.76 mmol) were reacted in MeOH/ $CH_2Cl_2$  (7 mL) according to the general procedure for the U-4CR. Flash column chromatography afforded TFAH **10a** (90 mg, 19%) as an orange foam:  $R_f = 0.18$  ( $CH_2Cl_2$ /MeOH/aqueous 30%  $NH_3$  92:8:0.1);  $^1H$  NMR (300 MHz,  $CD_3OD$ ):  $\delta = 8.09$  and  $8.04$  (d,  $J = 8.5$  Hz, 1H), 7.74–7.71 (m, 1H), 7.54 (d,  $J = 6.2$  Hz, 1H), 7.49 (d,  $J = 6.2$  Hz, 1H), 7.35–7.27 (m, 1H), 7.24–7.21 (m, 1H), 7.15–7.06 (m, 3H), 7.01–6.98 (m, 1H), 6.85 (d,  $J = 15.2$  Hz, 1H), 6.76 (t,  $J = 8.5$  Hz, 1H), 4.43 (s, 1H), 4.31 (s, 1H), 3.83 and 3.77 (m, 3H), 3.64–3.50 (m, 4H), 2.91 (m, 2H), 2.65–2.62 (m, 2H), 2.25–2.18 (m, 3H), 1.82 (m, 4H), 1.67–1.60 (m, 4H), 1.48–1.40 ppm (m, 2H);  $^{13}C$  NMR (75 MHz,  $CD_3OD$ ):  $\delta = 170.5$ , 170.3, 170.1, 157.9, 154.1, 150.8, 149.6, 146.5, 145.1, 140.2, 139.9, 134.3, 133.7, 130.6, 130.3, 129.8, 129.5, 128.4, 128.3, 128.2, 126.7, 125.2, 125.0, 124.8, 124.0, 123.6, 120.7, 116.8, 115.3, 114.9, 112.2, 111.9, 56.6, 52.1, 51.3, 50.7, 33.4, 32.0, 30.9, 30.0, 28.6, 26.0, 25.4, 25.2, 24.0, 23.5, 19.0 ppm; HPLC:  $t_R = 1.84$  min, 97.8%; HRMS ESI-TOF  $[M+H]^+$   $m/z$  calcd for  $C_{37}H_{41}ClN_4O_4$ : 641.2889, found: 641.2881.

**(*E*)-*N*-(2-((2-Chloro-6-methylphenyl)amino)-2-oxoethyl)-3-(4-hydroxy-3-methoxyphenyl)-*N*-(6-((1,2,3,4-tetrahydroacridin-9-yl)amino)hexyl)acrylamide (**10b**):** *N*'-(1,2,3,4-tetrahydroacridin-9-yl)hexane-1,6-diamine (**9b**) (206 mg, 0.69 mmol), paraformaldehyde (21 mg, 0.69 mmol), ferulic acid (134 mg, 0.69 mmol) and 2-chloro-6-methylphenylisocyanide (97 mg, 0.69 mmol) were reacted in MeOH/ $CH_2Cl_2$  (7 mL) according to the general procedure for the U-4CR. Flash column chromatography afforded TFAH **10b** (122 mg, 27%) as an orange foam:  $R_f = 0.16$  ( $CH_2Cl_2$ /MeOH/aqueous 30%  $NH_3$  92:8:0.1);  $^1H$  NMR (300 MHz,  $CD_3OD$ ):  $\delta = 8.05$  (t,  $J = 8.0$  Hz, 1H), 7.71 (d,  $J = 8.0$  Hz, 1H), 7.51 (d,  $J = 3.3$  Hz, 1H), 7.46 (d,  $J = 3.3$  Hz, 1H), 7.35–7.28 (m, 1H), 7.24–7.21 (m, 1H), 7.12–7.07 (m, 3H), 6.99 (t,  $J = 8.0$  Hz, 1H), 6.84 (d,  $J = 15.0$  Hz, 1H), 6.77–6.71 (m, 1H), 4.42 (s, 1H), 4.29 (s, 1H), 3.81 and 3.78 (s, 3H), 3.58–3.49 (m, 4H), 2.90 (m, 2H), 2.66–2.62 (m, 2H), 2.23 and 2.12 (s, 3H), 1.82 (m, 4H), 1.61 (m, 4H), 1.35–1.24 ppm (m, 4H);  $^{13}C$  NMR (75 MHz,



CD<sub>3</sub>OD):  $\delta$  = 170.4, 170.2 (2C), 170.0, 158.4, 153.9, 150.9, 149.6, 147.1, 145.2, 145.1, 140.1, 139.8, 134.3, 133.7, 130.3, 129.7, 129.5, 128.4, 128.3, 128.2, 127.3, 127.2, 125.0, 124.8, 124.7, 124.0, 123.6, 121.0, 116.8, 116.7, 116.5, 115.3, 114.8, 112.2, 111.8, 56.6, 52.0, 51.2, 50.8, 33.8, 32.2, 30.2, 28.7, 27.8, 27.5, 26.1, 24.1, 23.6, 19.0 ppm; IR (ATR):  $\tilde{\nu}_{\text{max}}$  = 3198, 2932, 2858, 1683, 1642, 1578, 1511, 1452, 1423 cm<sup>-1</sup>, 1364; HPLC:  $t_{\text{R}}$  = 2.15 min, 96.7%; HRMS ESI-TOF  $[M+H]^+$   $m/z$  calcd for C<sub>38</sub>H<sub>44</sub>ClN<sub>4</sub>O<sub>4</sub>: 655.3046, found: 655.3031.

**(E)-N-(2-((2-Chloro-6-methylphenyl)amino)-2-oxoethyl)-3-(4-hydroxy-3-methoxyphenyl)-N-(7-((1,2,3,4-tetrahydroacridin-9-yl)amino)heptyl)acrylamide (10c):** N<sup>1</sup>-(1,2,3,4-tetrahydroacridin-9-yl)-heptane-1,7-diamine (**9c**) (206 mg, 0.69 mmol), paraformaldehyde (21 mg, 0.69 mmol), ferulic acid (134 mg, 0.69 mmol) and 2-chloro-6-methylphenylisocyanide (97 mg, 0.69 mmol) were reacted in MeOH/CH<sub>2</sub>Cl<sub>2</sub> (7 mL) according to the general procedure for the U-4CR. Flash column chromatography afforded TFAH **10c** (122 mg, 27%) as a yellow foam:  $R_{\text{f}}$  = 0.25 (CH<sub>2</sub>Cl<sub>2</sub>/MeOH/aqueous 30% NH<sub>3</sub> 92:8:0.1); <sup>1</sup>H NMR (300 MHz, CD<sub>3</sub>OD):  $\delta$  = 8.05 (t,  $J$  = 9.1 Hz, 1H), 7.71 (d,  $J$  = 7.9 Hz, 1H), 7.51 (d,  $J$  = 4.9 Hz, 1H), 7.46 (d,  $J$  = 4.9 Hz, 1H), 7.32–7.27 (m, 1H), 7.22–7.20 (m, 1H), 7.11–7.08 (m, 3H), 6.99 (t,  $J$  = 9.1 Hz, 1H), 6.83 (d,  $J$  = 15.1 Hz, 1H), 6.77–6.71 (m, 1H), 4.41 (s, 1H), 4.29 (s, 1H), 3.79 (s, 3H), 3.57–3.46 (m, 4H), 2.90 (m, 2H), 2.62 (m, 2H), 2.23 and 2.16 (m, 3H), 1.82 (m, 4H), 1.60–1.57 (m, 4H), 1.30 ppm (m, 6H); <sup>13</sup>C NMR (75 MHz, CD<sub>3</sub>OD):  $\delta$  = 170.4, 170.2, 170.1, 170.0, 158.4, 153.7, 151.0, 149.6, 147.2, 145.1, 140.1, 139.8, 134.2, 133.6, 130.3, 129.7, 129.5, 128.4, 128.3, 128.1, 127.3, 125.0, 124.7, 124.0, 123.6, 121.0, 116.8, 116.4, 115.2, 114.7, 112.2, 111.8, 56.6, 52.0, 51.2, 50.8, 33.8, 32.3, 30.2, 28.7, 27.9, 27.7, 26.1, 24.1, 23.6, 19.0 ppm; IR (ATR):  $\tilde{\nu}_{\text{max}}$  = 3234, 2928, 2855, 1676, 1642, 1567, 1511, 1421 cm<sup>-1</sup>, 1367; HPLC:  $t_{\text{R}}$  = 2.95 min, 99.3%; HRMS ESI-TOF  $[M+H]^+$   $m/z$  calcd for C<sub>39</sub>H<sub>46</sub>ClN<sub>4</sub>O<sub>4</sub>: 669.3202, found: 669.3182.

**(E)-N-(2-((2-Chloro-6-methylphenyl)amino)-2-oxoethyl)-3-(4-hydroxy-3-methoxyphenyl)-N-(8-((1,2,3,4-tetrahydroacridin-9-yl)amino)octyl)acrylamide (10d):** N<sup>1</sup>-(1,2,3,4-tetrahydroacridin-9-yl)octane-1,8-diamine (**9d**) (243 mg, 0.75 mmol), paraformaldehyde (22 mg, 0.75 mmol), ferulic acid (134 mg, 0.75 mmol) and 2-chloro-6-methylphenylisocyanide (114 mg, 0.75 mmol) were reacted in MeOH/CH<sub>2</sub>Cl<sub>2</sub> (7 mL) according to the general procedure for the U-4CR. Flash column chromatography afforded TFAH **10d** (138 mg, 27%) as an orange foam:  $R_{\text{f}}$  = 0.30 (CH<sub>2</sub>Cl<sub>2</sub>/MeOH/aqueous 30% NH<sub>3</sub> 92:8:0.1); <sup>1</sup>H NMR (300 MHz, CD<sub>3</sub>OD):  $\delta$  = 8.05 (t,  $J$  = 8.0 Hz, 1H), 7.71 (d,  $J$  = 8.0 Hz, 1H), 7.51 (d,  $J$  = 6.0 Hz, 1H), 7.47 (d,  $J$  = 6.0 Hz, 1H), 7.31 (t,  $J$  = 8.0 Hz, 1H), 7.21 (m, 1H), 7.11–7.09 (m, 3H), 6.99 (t,  $J$  = 9.2 Hz, 1H), 6.84 (d,  $J$  = 15.1 Hz, 1H), 6.77–6.72 (m, 1H), 4.42 (s, 1H), 4.30 (s, 1H), 3.80 (s, 3H), 3.59–3.46 (m, 4H), 2.91 (m, 2H), 2.64 (m, 2H), 2.23 and 2.17 (m, 3H), 1.83 (m, 4H), 1.60–1.56 (m, 4H), 1.26 ppm (m, 8H); <sup>13</sup>C NMR (75 MHz, CD<sub>3</sub>OD):  $\delta$  = 170.5, 170.1, 170.0, 158.5, 153.7, 151.0, 149.6, 147.3, 145.1, 140.1, 139.8, 134.3, 134.1, 133.7, 130.2, 129.7, 129.5, 128.4, 128.3, 128.1, 127.4, 125.0, 124.7, 124.0, 123.6, 121.1, 116.9, 116.8, 116.5, 115.3, 114.8, 112.3, 111.8, 56.6, 52.0, 51.2, 50.8, 33.9, 32.3, 30.3, 30.2, 28.8, 27.9, 27.6, 26.1, 24.1, 23.7, 19.0 ppm; IR (ATR):  $\tilde{\nu}_{\text{max}}$  = 3193, 2927, 2854, 1676, 1642, 1578, 1511, 1452, 1365 cm<sup>-1</sup>; HPLC:  $t_{\text{R}}$  = 3.63 min, 98.3%; HRMS ESI-TOF  $[M+H]^+$   $m/z$  calcd for C<sub>40</sub>H<sub>48</sub>ClN<sub>4</sub>O<sub>4</sub>: 683.3359, found: 683.3342.

**(E)-N-(2-((2-Chloro-6-methylphenyl)amino)-2-oxoethyl)-3-(4-hydroxy-3-methoxyphenyl)-N-(9-((1,2,3,4-tetrahydroacridin-9-yl)amino)nonyl)acrylamide (10e):** N<sup>1</sup>-(1,2,3,4-tetrahydroacridin-9-yl)nonane-1,9-diamine (**9e**) (204 mg, 0.60 mmol), paraformaldehyde (18 mg, 0.60 mmol), ferulic acid (117 mg, 0.60 mmol) and 2-chloro-6-methylphenylisocyanide (91 mg, 0.60 mmol) were reacted in MeOH/CH<sub>2</sub>Cl<sub>2</sub> (7 mL) according to the general procedure for the U-

4CR. Flash column chromatography afforded TFAH **10e** (78 mg, 19%) as an orange foam:  $R_{\text{f}}$  = 0.29 (CH<sub>2</sub>Cl<sub>2</sub>/MeOH/aqueous 30% NH<sub>3</sub> 92:8:0.1); <sup>1</sup>H NMR (300 MHz, CD<sub>3</sub>OD):  $\delta$  = 8.06 (t,  $J$  = 8.4 Hz, 1H), 7.74 (d,  $J$  = 8.4 Hz, 1H), 7.56–7.49 (m, 2H), 7.32 (t,  $J$  = 8.4 Hz, 1H), 7.25–7.22 (m, 1H), 7.15–6.98 (m, 4H), 6.86 (d,  $J$  = 15.0 Hz, 1H), 6.80–6.74 (m, 1H), 4.45 (s, 1H), 4.34 (s, 1H), 3.83 (s, 3H), 3.62–3.60 (m, 1H), 3.53–3.44 (m, 3H), 2.93 (m, 2H), 2.66 (m, 2H), 2.26 and 2.20 (m, 3H), 1.85 (m, 4H), 1.65–1.57 (m, 4H), 1.28–1.20 ppm (m, 10H); <sup>13</sup>C NMR (75 MHz, CD<sub>3</sub>OD):  $\delta$  = 170.5, 170.2, 170.0, 158.8, 153.6, 151.3, 149.7, 147.6, 145.1, 140.1, 133.7, 130.3, 130.1, 129.7, 129.5, 128.3, 128.0, 127.7, 124.9, 124.7, 124.0, 123.7, 121.2, 116.9, 116.8, 116.6, 115.2, 114.7, 112.2, 111.8, 56.6, 52.0, 51.2, 50.8, 34.0, 32.4, 30.5, 30.4, 28.0, 27.7, 26.2, 24.2, 23.7, 19.0 ppm; HPLC:  $t_{\text{R}}$  = 4.74 min, 96.9%; HRMS ESI-TOF  $[M+H]^+$   $m/z$  calcd for C<sub>41</sub>H<sub>50</sub>ClN<sub>4</sub>O<sub>4</sub>: 697.3515, found: 697.3491.

**(E)-N-(2-(Benzylamino)-2-oxoethyl)-3-(4-hydroxy-3-methoxyphenyl)-N-(6-((1,2,3,4-tetrahydroacridin-9-yl)amino)hexyl)acrylamide (10f):** N<sup>1</sup>-(1,2,3,4-tetrahydroacridin-9-yl)hexane-1,6-diamine (**9b**) (200 mg, 0.67 mmol), paraformaldehyde (20 mg, 0.67 mmol), ferulic acid (130 mg, 0.67 mmol) and benzylisocyanide (82  $\mu$ L, 0.67 mmol) were reacted in MeOH/CH<sub>2</sub>Cl<sub>2</sub> (7 mL) according to the general procedure for the U-4CR. Flash column chromatography afforded TFAH **10f** (139 mg, 33%) as a yellow foam:  $R_{\text{f}}$  = 0.25 (CH<sub>2</sub>Cl<sub>2</sub>/MeOH/aqueous 30% NH<sub>3</sub> 92:8:0.1); <sup>1</sup>H NMR (300 MHz, CD<sub>3</sub>OD):  $\delta$  = 8.08–8.01 (m, 1H), 7.65 (m, 1H), 7.51 (m, 1H), 7.42 (d,  $J$  = 15.0 Hz, 1H), 7.31 (m, 1H), 7.20–7.08 (m, 5H), 7.00–6.85 (m, 2H), 6.78 (d,  $J$  = 15.0 Hz, 1H), 6.69–6.61 (m, 1H), 4.32 (m, 2H), 4.18 (s, 1H), 4.07 (s, 1H), 3.73 and 3.70 (m, 3H), 3.49 (m, 2H), 2.85 (m, 2H), 2.58–2.55 (m, 2H), 1.77 (m, 4H), 1.57–1.47 (m, 4H), 1.28–1.20 ppm (m, 6H); <sup>13</sup>C NMR (75 MHz, CD<sub>3</sub>OD):  $\delta$  = 171.4, 171.2, 169.9, 169.8, 157.1, 156.9, 156.8, 156.7, 154.7, 154.5, 150.6, 149.4, 145.5, 145.4, 144.9, 140.0, 131.1, 129.6, 128.6, 128.3, 128.2, 125.8, 125.6, 125.3, 125.2, 125.1, 123.7, 123.6, 123.5, 120.1, 116.7, 115.7, 115.5, 115.3, 114.9, 112.2, 112.0, 56.6, 52.2, 51.4, 50.7, 49.6, 44.3, 44.2, 44.0, 32.8, 32.1, 30.9, 30.2, 28.6, 27.7, 27.4, 25.8, 23.8, 23.2 ppm; HPLC:  $t_{\text{R}}$  = 1.73 min, 97.6%; HRMS ESI-TOF  $[M+H]^+$   $m/z$  calcd for C<sub>38</sub>H<sub>45</sub>N<sub>4</sub>O<sub>4</sub>: 621.3435, found: 621.3435.

**(E)-N-(2-(Benzylamino)-2-oxoethyl)-3-(4-hydroxy-3-methoxyphenyl)-N-(7-((1,2,3,4-tetrahydroacridin-9-yl)amino)heptyl)acrylamide (10g):** N<sup>1</sup>-(1,2,3,4-tetrahydroacridin-9-yl)heptane-1,7-diamine (**9c**) (168 mg, 0.54 mmol), paraformaldehyde (16 mg, 0.54 mmol), ferulic acid (105 mg, 0.54 mmol) and benzylisocyanide (66  $\mu$ L, 0.67 mmol) were reacted in MeOH/CH<sub>2</sub>Cl<sub>2</sub> (7 mL) according to the general procedure for the U-4CR. Flash column chromatography CH<sub>2</sub>Cl<sub>2</sub>/MeOH/aqueous 30% NH<sub>3</sub> (92:8:0.1) afforded TFAH **10g** (165 mg, 48%) as a yellow foam:  $R_{\text{f}}$  = 0.30 (CH<sub>2</sub>Cl<sub>2</sub>/MeOH/aqueous 30% NH<sub>3</sub> 92:8:0.1); <sup>1</sup>H NMR (300 MHz, CD<sub>3</sub>OD):  $\delta$  = 8.13–8.06 (m, 1H), 7.75–7.73 (m, 1H), 7.57–7.47 (m, 2H), 7.40–6.96 (m, 8H), 6.89–6.65 (m, 2H), 4.39 (m, 2H), 4.23 (s, 1H), 4.12 (s, 1H), 3.84 and 3.80 (m, 3H), 3.55–3.44 (m, 4H), 2.96 (m, 2H), 2.72–2.70 (m, 2H), 1.89 (m, 4H), 1.62 (m, 4H), 1.34–1.29 ppm (m, 6H); <sup>13</sup>C NMR (75 MHz, CD<sub>3</sub>OD):  $\delta$  = 171.4, 171.2, 169.9, 169.8, 158.2, 153.8, 153.7, 151.3, 149.6, 146.9, 145.0, 140.0 (2C), 139.9, 130.4, 129.6, 128.7, 128.6, 128.3 (2C), 127.9, 127.1, 125.0, 124.7, 123.8, 123.6, 120.8, 116.9, 116.8, 116.3, 115.1, 114.7, 112.2, 112.1, 56.6, 52.2, 51.4, 50.7, 44.3 (2C), 44.2, 44.0, 33.6, 32.2, 30.1, 28.6, 28.3, 27.9, 27.6, 26.0, 24.0, 23.5, 23.4, 23.3 ppm; IR (ATR):  $\tilde{\nu}_{\text{max}}$  = 3284, 2928, 2855, 1642, 1579, 1511, 1452, 1423 cm<sup>-1</sup>; HPLC:  $t_{\text{R}}$  = 1.63 min, 95.1%; HRMS ESI-TOF  $[M+H]^+$   $m/z$  calcd for C<sub>39</sub>H<sub>47</sub>N<sub>4</sub>O<sub>4</sub>: 635.3592, found: 635.3577.

**(E)-N-(2-(Benzylamino)-2-oxoethyl)-3-(4-hydroxy-3-methoxyphenyl)-N-(8-((1,2,3,4-tetrahydroacridin-9-yl)amino)octyl)acrylamide (10h):** N<sup>1</sup>-(1,2,3,4-tetrahydroacridin-9-yl)octane-1,8-diamine

(**9d**) (176 mg, 0.54 mmol), paraformaldehyde (16 mg, 0.54 mmol), ferulic acid (105 mg, 0.54 mmol) and benzyliisocyanide (66  $\mu$ L, 0.67 mmol) were reacted in MeOH/CH<sub>2</sub>Cl<sub>2</sub> (7 mL) according to the general procedure for the U-4CR. Flash column chromatography CH<sub>2</sub>Cl<sub>2</sub>/MeOH/aqueous 30% NH<sub>3</sub> (92:8:0.1) afforded TFAH **10h** (95 mg, 27%) as a yellow foam:  $R_f$ =0.31 (CH<sub>2</sub>Cl<sub>2</sub>/MeOH/aqueous 30% NH<sub>3</sub> 92:8:0.1); <sup>1</sup>H NMR (300 MHz, CD<sub>3</sub>OD):  $\delta$ =8.28–8.20 (m, 1H), 7.71 (m, 2H), 7.49–7.44 (m, 2H), 7.28–7.10 (m, 6H), 7.05–7.00 (m, 1H), 6.94–6.84 (m, 1H), 6.74–6.66 (m, 1H), 4.38–4.35 (m, 2H), 4.25 (s, 1H), 4.12 (s, 1H), 3.83–3.71 (m, 5H), 3.58–3.53 (m, 1H), 3.48–3.44 (m, 1H), 3.19 (s, 1H), 2.95 (m, 2H), 2.66 (m, 2H), 1.90 (m, 4H), 1.74–1.54 (m, 4H), 1.33 ppm (m, 8H); <sup>13</sup>C NMR (75 MHz, CD<sub>3</sub>OD):  $\delta$ =171.5, 171.3, 170.0 (2C), 158.7, 153.7, 151.0, 149.7, 147.5, 145.0, 140.0, 130.2, 129.8, 129.7, 128.7, 128.3, 128.1, 127.6, 124.9, 124.7, 123.8, 123.6, 121.1, 116.9, 116.8, 116.6, 115.2 (2C), 114.8, 112.2, 112.1, 56.6, 52.3, 51.4, 50.7, 44.4, 44.2, 34.0, 32.3, 30.3, 30.2, 28.7, 27.9, 27.6, 26.2, 24.1, 23.7, 23.6, 23.5 ppm; IR (ATR):  $\tilde{\nu}_{\max}$ =3233, 3059, 2927, 2854, 1638, 1584, 1514, 1452, 1427 cm<sup>-1</sup>; HPLC:  $t_R$ =2.71 min, 95.7%; HRMS ESI-TOF [ $M+H$ ]<sup>+</sup>  $m/z$  calcd for C<sub>40</sub>H<sub>49</sub>N<sub>4</sub>O<sub>4</sub>: 649.3748, found: 649.3736.

(**E**)-3-(4-Hydroxy-3-methoxyphenyl)-*N*-(2-(naphthalen-2-ylamino)-2-oxoethyl)-*N*-(6-((1,2,3,4-tetrahydroacridin-9-yl)amino)hexyl)acrylamide (**10i**): *N*<sup>1</sup>-(1,2,3,4-tetrahydroacridin-9-yl)hexane-1,6-diamine (**9b**) (200 mg, 0.67 mmol), paraformaldehyde (20 mg, 0.67 mmol), ferulic acid (130 mg, 0.67 mmol) and naphthylisocyanide (103 mg, 0.67 mmol) were reacted in MeOH/CH<sub>2</sub>Cl<sub>2</sub> (7 mL) according to the general procedure for the U-4CR. Flash column chromatography afforded TFAH **10i** (143 mg, 32%) as a pale-brown foam:  $R_f$ =0.17 (CH<sub>2</sub>Cl<sub>2</sub>/MeOH/aqueous 30% NH<sub>3</sub> 92:8:0.1); <sup>1</sup>H NMR (300 MHz, CD<sub>3</sub>OD):  $\delta$ =8.17 (m, 1H), 8.09–8.02 (m, 1H), 7.71–7.64 (m, 4H), 7.54–7.50 (m, 3H), 7.38–7.32 (m, 3H), 7.09–6.69 (m, 4H), 4.42 (s, 1H), 4.26 (s, 1H), 3.79 (m, 2H), 3.67–3.60 (m, 1H), 3.52–3.48 (m, 2H), 2.89 (m, 2H), 2.59 (m, 2H), 1.80 (m, 4H), 1.62–1.56 (m, 4H), 1.37 ppm (m, 6H); <sup>13</sup>C NMR (75 MHz, CD<sub>3</sub>OD):  $\delta$ =170.0, 169.8, 157.8, 154.1, 150.8, 149.5, 146.5, 145.2, 144.9, 137.3, 135.3, 132.3, 132.2, 130.6, 129.8, 129.7, 128.7, 128.6, 128.3, 128.2, 127.6, 126.6, 126.4, 126.2, 126.1, 125.1, 125.0, 124.8, 123.9, 123.8, 121.3, 121.2, 120.6, 118.0, 117.9, 116.8, 116.7, 116.2, 115.6, 114.8, 112.2, 111.7, 56.6, 52.8, 52.3, 50.9, 49.6, 33.4, 32.1, 32.1, 30.9, 30.3, 28.8, 27.9, 27.7, 27.4, 25.9, 23.9, 23.4, 23.3 ppm; IR (ATR):  $\tilde{\nu}_{\max}$ =3269, 2928, 2855, 1690, 1640, 1583, 1561, 1503, 1418, 1361 cm<sup>-1</sup>; HPLC:  $t_R$ =3.31 min, 98.1%; HRMS ESI-TOF [ $M+H$ ]<sup>+</sup>  $m/z$  calcd for C<sub>41</sub>H<sub>45</sub>N<sub>4</sub>O<sub>4</sub>: 657.3435, found: 657.3434.

(**E**)-3-(4-Hydroxy-3-methoxyphenyl)-*N*-(2-(naphthalen-2-ylamino)-2-oxoethyl)-*N*-(7-((1,2,3,4-tetrahydroacridin-9-yl)amino)heptyl)acrylamide (**10j**): *N*<sup>1</sup>-(1,2,3,4-tetrahydroacridin-9-yl)heptane-1,7-diamine (**9c**) (200 mg, 0.64 mmol), paraformaldehyde (19 mg, 0.64 mmol), ferulic acid (124 mg, 0.64 mmol) and naphthylisocyanide (98 mg, 0.64 mmol) were reacted in MeOH/CH<sub>2</sub>Cl<sub>2</sub> (7 mL) according to the general procedure for the U-4CR. Flash column chromatography afforded TFAH **10j** (131 mg, 30%) as an orange-brown foam:  $R_f$ =0.19 (CH<sub>2</sub>Cl<sub>2</sub>/MeOH/aqueous 30% NH<sub>3</sub> 92:8:0.1); <sup>1</sup>H NMR (300 MHz, CD<sub>3</sub>OD):  $\delta$ =8.17 (m, 1H), 8.04 (m, 1H), 7.69 (m, 4H), 7.53–7.50 (m, 3H), 7.35–7.32 (m, 3H), 7.09–6.68 (m, 4H), 4.42 (s, 1H), 4.27 (s, 1H), 3.80 and 3.67 (s, 3H), 3.60 (m, 1H), 3.47 (m, 3H), 2.90 (m, 2H), 2.61 (m, 2H), 1.82 (m, 4H), 1.62–1.56 (m, 4H), 1.30–1.26 ppm (m, 6H); <sup>13</sup>C NMR (75 MHz, CD<sub>3</sub>OD):  $\delta$ =170.0, 169.8, 157.5, 154.2, 150.8, 149.6, 146.2, 145.2, 144.8, 144.8, 144.7, 137.3, 136.5, 135.3, 132.2, 130.8, 130.7, 129.7, 128.7, 128.2, 127.6, 126.6, 126.4, 126.3, 126.2, 125.2, 125.0, 124.6, 123.9, 123.6, 121.3, 120.4, 120.2, 118.0, 117.9, 117.7, 116.8, 116.4, 116.0, 115.6, 114.8, 113.4, 113.2, 112.3, 111.7, 56.6, 52.8, 52.3, 51.0, 33.3, 32.1, 30.9, 30.2, 29.3,

27.9, 27.7, 25.9, 23.9, 23.4, 23.3 ppm; IR (ATR):  $\tilde{\nu}_{\max}$ =3280, 2927, 2854, 1690, 1639, 1583, 1560, 1503, 1432, 1361 cm<sup>-1</sup>; HPLC:  $t_R$ =4.02 min, 95.6%; HRMS ESI-TOF [ $M+H$ ]<sup>+</sup>  $m/z$  calcd for C<sub>42</sub>H<sub>47</sub>N<sub>4</sub>O<sub>4</sub>: 671.3592, found: 671.3580.

(**E**)-3-(4-Hydroxy-3-methoxyphenyl)-*N*-(2-(naphthalen-2-ylamino)-2-oxoethyl)-*N*-(8-((1,2,3,4-tetrahydroacridin-9-yl)amino)octyl)acrylamide (**10k**): *N*<sup>1</sup>-(1,2,3,4-tetrahydroacridin-9-yl)octane-1,8-diamine (**9d**) (200 mg, 0.61 mmol), paraformaldehyde (18 mg, 0.61 mmol), ferulic acid (118 mg, 0.61 mmol) and naphthylisocyanide (93 mg, 0.61 mmol) were reacted in MeOH/CH<sub>2</sub>Cl<sub>2</sub> (7 mL) according to the general procedure for the U-4CR. Flash column chromatography afforded TFAH **10k** (74 mg, 18%) as an orange-brown foam:  $R_f$ =0.32 (CH<sub>2</sub>Cl<sub>2</sub>/MeOH/aqueous 30% NH<sub>3</sub> 92:8:0.1); <sup>1</sup>H NMR (300 MHz, CD<sub>3</sub>OD):  $\delta$ =8.20–8.18 (m, 1H), 8.08–8.04 (m, 1H), 7.75–7.68 (m, 4H), 7.56–7.49 (m, 3H), 7.40–7.34 (m, 3H), 7.14–6.70 (m, 4H), 4.44 (s, 1H), 4.29 (s, 1H), 3.83 and 3.69 (s, 3H), 3.64–3.59 (m, 1H), 3.50–3.45 (m, 3H), 2.93 (m, 2H), 2.65 (m, 2H), 1.85 (m, 4H), 1.65–1.56 (m, 4H), 1.27 ppm (m, 8H); <sup>13</sup>C NMR (75 MHz, CD<sub>3</sub>OD):  $\delta$ =170.1, 169.9, 154.0, 150.8, 150.1, 149.6, 146.9, 145.2, 144.8, 135.4, 132.3, 130.5, 129.8, 129.7, 129.6, 128.7, 128.3, 127.6, 127.0, 126.1, 125.1, 124.8, 123.6, 121.3, 121.3, 120.9, 118.2, 118.0, 116.8, 116.7, 116.4, 115.7, 114.9, 112.3, 111.7, 56.6, 52.8, 52.2, 51.0, 33.6, 32.2, 30.3, 28.8, 27.8, 27.6, 26.0, 24.1, 23.6, 23.5 ppm; IR (ATR):  $\tilde{\nu}_{\max}$ =3200, 2928, 2856, 1689, 1638, 1560, 1504, 1431, 1352; HPLC:  $t_R$ =5.57 min, 98.9%; HRMS ESI-TOF [ $M+H$ ]<sup>+</sup>  $m/z$  calcd for C<sub>43</sub>H<sub>49</sub>N<sub>4</sub>O<sub>4</sub>: 685.3748, found: 685.3744.

(**E**)-*N*-(2-((2-Chloro-6-methylphenyl)amino)-2-oxoethyl)-3-(4-hydroxy-3-methoxyphenyl)-*N*-(8-((7-methoxy-1,2,3,4-tetrahydroacridin-9-yl)amino)octyl)acrylamide (**10l**): *N*<sup>1</sup>-(7-methoxy-1,2,3,4-tetrahydroacridin-9-yl)octane-1,8-diamine (**9f**) (202 mg, 0.57 mmol), paraformaldehyde (17 mg, 0.57 mmol), ferulic acid (110 mg, 0.57 mmol) and 2-chloro-6-methylphenylisocyanide (86 mg, 0.57 mmol) were reacted in MeOH/CH<sub>2</sub>Cl<sub>2</sub> (7 mL) according to the general procedure for the U-4CR. Flash column chromatography afforded TFAH **10l** (64 mg, 16%) as a pale-brown foam:  $R_f$ =0.20 (CH<sub>2</sub>Cl<sub>2</sub>/MeOH/aqueous 30% NH<sub>3</sub> 92:8:0.1); <sup>1</sup>H NMR (300 MHz, CD<sub>3</sub>OD):  $\delta$ =7.67 (d,  $J$ =9.0 Hz, 1H), 7.52 (d,  $J$ =15.2 Hz, 1H), 7.36 (d,  $J$ =7.1 Hz, 1H), 7.28–7.21 (m, 2H), 7.18–7.12 (m, 3H), 7.03 (t,  $J$ =9.0 Hz, 1H), 6.91–6.81 (m, 1H), 6.76 (d,  $J$ =8.1 Hz, 1H), 4.46–4.32 (m, 2H), 3.88–3.72 (m, 6H), 3.63–3.40 (m, 4H), 2.93 (m, 2H), 2.73–2.71 (m, 2H), 2.26 and 2.20 (s, 3H), 1.86 (m, 4H), 1.68–1.59 (m, 4H), 1.31–1.26 ppm (m, 8H); <sup>13</sup>C NMR (75 MHz, CD<sub>3</sub>OD):  $\delta$ =172.6, 170.5, 157.8, 156.7, 152.8, 150.7, 149.6, 145.1, 143.1, 140.1, 136.2, 134.3, 133.7, 130.4, 130.3, 129.8, 129.7 (2C), 129.5, 129.2, 129.1, 128.4 (2C), 124.3, 124.0, 123.8, 123.6, 122.4, 122.3, 118.1, 118.0, 116.8, 116.7, 116.3, 115.4, 115.0, 113.2, 112.3, 111.9, 103.2, 56.6, 56.3, 51.6, 51.2, 50.8, 33.8, 32.4, 30.4, 30.4, 30.2, 28.0, 27.7, 27.6, 26.4, 24.2, 23.8, 23.7, 19.0 ppm; IR (ATR):  $\tilde{\nu}_{\max}$ =3234, 2928, 2855, 1679, 1625, 1581, 1505, 1452, 1429 cm<sup>-1</sup>; HPLC:  $t_R$ =4.10 min, 95.6%; HRMS ESI-TOF [ $M+H$ ]<sup>+</sup>  $m/z$  calcd for C<sub>41</sub>H<sub>50</sub>ClN<sub>4</sub>O<sub>5</sub>: 713.3464, found: 713.3471.

(**E**)-*N*-(2-(Benzylamino)-2-oxoethyl)-3-(4-hydroxy-3-methoxyphenyl)-*N*-(8-((7-methoxy-1,2,3,4-tetrahydroacridin-9-yl)amino)octyl)acrylamide (**10m**): *N*<sup>1</sup>-(7-methoxy-1,2,3,4-tetrahydroacridin-9-yl)octane-1,8-diamine (**9f**) (202 mg, 0.57 mmol), paraformaldehyde (17 mg, 0.57 mmol), ferulic acid (110 mg, 0.57 mmol) and benzyliisocyanide (70  $\mu$ L, 0.57 mmol) were reacted in MeOH/CH<sub>2</sub>Cl<sub>2</sub> (7 mL) according to the general procedure for the U-4CR. Flash column chromatography afforded TFAH **10m** (97 mg, 25%) as a yellow foam:  $R_f$ =0.23 (CH<sub>2</sub>Cl<sub>2</sub>/MeOH/aqueous 30% NH<sub>3</sub> 98:2:0.1); <sup>1</sup>H NMR (300 MHz, CD<sub>3</sub>OD):  $\delta$ =7.60 (d,  $J$ =9.0 Hz, 1H), 7.46–7.39 (m, 1H), 7.28–7.25 (m, 1H), 7.21–7.19 (m, 2H), 7.16–7.11 (m, 3H),



7.07–7.05 (m, 1H), 7.02 (m, 1H), 6.97–6.93 (m, 1H), 6.88–6.59 (m, 2H), 4.31 and 4.29 (s, 2H), 4.16 (s, 1H), 4.06 (s, 1H), 3.79–3.68 (m, 6H), 3.46–3.41 (m, 2H), 3.37–3.26 (m, 2H), 2.84 (m, 2H), 2.62–2.60 (m, 2H), 1.76 (m, 4H), 1.48 (m, 4H), 1.17 ppm (m, 8H);  $^{13}\text{C}$  NMR (75 MHz,  $\text{CD}_3\text{OD}$ ):  $\delta$  = 171.4, 171.2, 169.9 (2C), 157.7, 156.6, 152.7, 151.0, 150.9, 149.6, 145.0, 143.1, 140.0, 139.9, 129.6, 129.1, 128.6, 128.3, (2C), 128.1, 123.8, 123.6, 122.3, 122.2, 117.9, 116.9, 116.8, 115.2, 114.8, 112.2, 112.1, 103.2, 56.6, 56.2, 52.2, 51.4, 50.7, 44.3, 44.2, 44.0, 33.8, 32.4, 30.4, 30.3, 30.2, 28.7, 28.0, 27.6, 26.3, 24.2, 23.8 ppm; IR (ATR):  $\tilde{\nu}_{\text{max}}$  = 3282, 2927, 2854, 1643, 1581, 1511, 1453, 1428  $\text{cm}^{-1}$ ; HPLC:  $t_{\text{R}}$  = 3.37 min, 96.0%; HRMS ESI-TOF  $[M+H]^+$   $m/z$  calcd for  $\text{C}_{41}\text{H}_{51}\text{N}_4\text{O}_5$ : 679.3854, found: 679.3868.

**(E)-3-(Hydroxy-3-methoxyphenyl)-N-(8((7-methoxy-1,2,3,4-tetrahydroacridin-9-yl)amino)octyl)-N-(2-(naphthalen-2-ylamino)2-oxoethyl)acrylamide (10n):**  $\text{N}^1$ -(7-methoxy-1,2,3,4-tetrahydroacridin-9-yl)octane-1,8-diamine (**9f**) (209 mg, 0.59 mmol), paraformaldehyde (18 mg, 0.59 mmol), ferulic acid (114 mg, 0.59 mmol) and naphthylisocyanide (90 mg, 0.59 mmol) were reacted in MeOH/ $\text{CH}_2\text{Cl}_2$  (7 mL) according to the general procedure for the U-4CR. Flash column chromatography afforded TFAH **10n** (74 mg, 18%) as a pale-brown foam:  $R_f$  = 0.30 ( $\text{CH}_2\text{Cl}_2/\text{MeOH}/\text{aqueous}$  30%  $\text{NH}_3$  92:8:0.1);  $^1\text{H}$  NMR (300 MHz,  $\text{CD}_3\text{OD}$ ):  $\delta$  = 8.18 (m, 1H), 7.75–7.63 (m, 4H), 7.55–7.48 (m, 2H), 7.38–7.29 (m, 3H), 7.24–7.18 (m, 1H), 7.11–6.67 (m, 4H), 4.42–4.17 (m, 2H), 3.85–3.67 (m, 6H), 3.61–3.33 (m, 4H), 2.89 (m, 2H), 2.67–2.65 (m, 2H), 1.83 (m, 4H), 1.62–1.55 (m, 4H), 1.32–1.25 ppm (m, 8H);  $^{13}\text{C}$  NMR (75 MHz,  $\text{CD}_3\text{OD}$ ):  $\delta$  = 170.0, 169.8, 157.8, 156.3 (2C), 152.9, 150.8, 149.6, 149.0, 145.2, 144.8, 137.3, 136.5, 135.3, 132.2, 129.8, 129.7, 128.9, 128.8, 128.7, 128.6, 128.3, 127.6 (2C), 126.1, 124.6, 123.8, 123.6, 122.3, 122.2, 121.3, 121.2, 121.1, 120.2, 118.0, 117.9, 116.8, 116.6, 116.2, 114.8, 113.3, 113.2, 112.3, 111.7, 103.3, 56.6, 56.3, 52.3, 51.7, 51.0, 33.6, 33.6, 32.4, 30.4, 30.3, 28.0, 27.7, 27.6, 26.3, 24.1, 23.7 ppm; IR (ATR):  $\tilde{\nu}_{\text{max}}$  = 3286, 2928, 2854, 1690, 1627, 1583, 1560, 1503, 1451, 1430  $\text{cm}^{-1}$ ; HPLC:  $t_{\text{R}}$  = 6.53 min, 97.4%; HRMS ESI-TOF  $[M+H]^+$   $m/z$  calcd for  $\text{C}_{44}\text{H}_{51}\text{N}_4\text{O}_5$ : 715.3854, found: 715.3830.

### Cell culture and biological assays

**In vitro toxicity of TFAHs 10a–n in HepG2 cells:** The HepG2 cell line was kindly provided by IdiPAZ Institute for Health Research (Madrid, Spain). The cells were cultured in Eagle's minimum essential medium (EMEM) supplemented with 15 nonessential amino acids, 1 mM sodium pyruvate, 10% heat-inactivated fetal bovine serum (FBS), 100  $\text{U mL}^{-1}$  penicillin, and 100  $\mu\text{g mL}^{-1}$  streptomycin (reagents from Invitrogen, Madrid, Spain). Cultures were seeded into flasks containing supplemented medium and maintained at 37 °C in a humidified atmosphere of 5%  $\text{CO}_2$  and 95% air. Culture media were changed every two days. Cells were sub-cultured after partial digestion with 0.25% trypsin–EDTA. For assays, HepG2 cells were sub-cultured in 96-well plates at a seeding density of  $1 \times 10^5$  cells per well. When the cells reached 80% confluence, the medium was replaced with fresh medium containing 1–1000  $\mu\text{M}$  compounds or 0.1% DMSO as a vehicle control. The cell viability was determined by MTT assay. The absorption was measured by a well plate reader at  $\lambda$  540 nm. All compounds were dissolved in pure DMSO, but the final DMSO concentration (1–1000  $\mu\text{M}$ ) was 0.1% in culture medium.

**Effect of TFAHs 10a–n on O/R- and  $\text{H}_2\text{O}_2$ -induced oxidative cell damage in SH-SY5Y cells:** Human dopaminergic neuroblastoma SH-SY5Y cells were maintained in a 1:1 mixture of Nutrient Mixture F-12 and EMEM supplemented with 15 nonessential amino acids, sodium pyruvate (1 mM), 10% heat-inactivated FBS, 100  $\text{U mL}^{-1}$

penicillin, and 100  $\mu\text{g mL}^{-1}$  streptomycin. Cultures were seeded into flasks containing supplemented medium and maintained at 37 °C in a humidified atmosphere of 5%  $\text{CO}_2$  and 95% air. For assays, SH-SY5Y cells were sub-cultured in 96-well plates at a seeding density of  $8 \times 10^4$  cells per well for two days. Cells were co-incubated with  $\text{H}_2\text{O}_2$  (300  $\mu\text{M}$ ) or oligomycin A (10  $\mu\text{M}$ )/rotenone (30  $\mu\text{M}$ ) (O/R) for 24 h to induce oxidative stress at several concentrations of test compounds in F-12/EMEM with 1% FBS. A vehicle group containing 0.1% DMSO was employed in parallel for each experiment. All SH-SY5Y cells used in this study were used at a low passage number (<13). The cell viability was determined by MTT assay. The absorption was measured by a well plate reader at  $\lambda$  540 nm.

**Effects of TFAHs 10a–n on  $\text{A}\beta_{1-40}$  and  $\text{A}\beta_{1-42}$  peptide-induced neurotoxicity in SH-SY5Y cells:** Lyophilized  $\text{A}\beta_{1-40}$  and  $\text{A}\beta_{1-42}$  peptides (Abcam, MA, USA) were reconstituted in sterile water at a concentration of 2 mM and kept at –80 °C until use. Aliquots were diluted with culture medium to achieve a final concentration of 30  $\mu\text{M}$  and then incubated at 37 °C for 72 h to form aggregated amyloid. For assays, SH-SY5Y cells were sub-cultured into a 96 well plate for 24 h. The cells were then incubated with  $\text{A}\beta_{1-40}$  and  $\text{A}\beta_{1-42}$  peptides (30  $\mu\text{M}$ ) with or without test compounds at various concentrations for 24 h. Cell viability was determined by MTT assay. The absorption was measured by a well plate reader at  $\lambda$  540 nm.

**Measurement of cell viability:** MTT reduction was performed as described<sup>[38]</sup> for the HepG2 cell line. This assay is based on the ability of the mitochondrial enzyme succinate dehydrogenase to convert the yellow water-soluble 3-(4,5-dimethylthiazol-2-yl)-2,5-diphenyltetrazolium bromide (MTT) into formazan crystals in metabolically active cells. Briefly, 50  $\mu\text{L}$  of the MTT labeling reagent, at a final concentration of 0.5  $\text{mg mL}^{-1}$ , was added. After incubation for 2 h, in a humidified incubator at 37 °C with 5%  $\text{CO}_2$  and 95% air (v/v), the supernatant was removed, and the obtained purple formazan product was re-suspended in 100  $\mu\text{L}$  DMSO. Colorimetric determination of MTT reduction was measured in an ELISA microplate reader at  $\lambda$  540 nm. Control cells treated with EMEM were taken as 100% viability.

**Inhibition of EeAChE and eqBuChE:** The inhibitory activity of the TFAHs on cholinesterases was determined by following the spectrophotometric method of Ellman et al.,<sup>[41]</sup> using purified AChE from *Electrophorus electricus* (Type V-S, Sigma–Aldrich) or BuChE from horse serum (lyophilized powder, Sigma–Aldrich). Enzymes were first dissolved in 0.1 M phosphate buffer (pH 8.0) and then aliquotted into small vials. Compound stock solutions in DMSO (10 mM) were further diluted with DMSO to prepare nine serial dilutions of each compound. The reactions were performed at a final volume of 3 mL in 0.1 M phosphate-buffered saline (PBS) at pH 8.0, containing 5,5'-dithiobis-2-nitrobenzoic acid (DTNB, 2625  $\mu\text{M}$ , 0.35 mM final concentration), EeAChE (29  $\mu\text{L}$ , 0.035  $\text{U mL}^{-1}$  final concentration) or eqBuChE (60  $\mu\text{L}$ , 0.05  $\text{U mL}^{-1}$  final concentration), test compound (3  $\mu\text{L}$ , 0.001–1000 nM final concentrations), and 1% w/v bovine serum albumin (BSA, 60  $\mu\text{L}$ ) in PBS (pH 8.0). Inhibition curves were built by pre-incubating this mixture at room temperature with nine concentrations of each compound for 10 min. A control with no compound was always present to determine the percent enzyme activity. After this pre-incubation period, acetylthiocholine iodide (105  $\mu\text{L}$ , 0.35 mM final concentration) or butyrylthiocholine iodide (150  $\mu\text{L}$ , 0.5 mM final concentration) was added, allowing 15 min of additional incubation time, during which the DTNB produces the yellow anion 5-thio-2-nitrobenzoic acid as an indicator of enzymatic activity. After 15 min, absorbance values were measured at  $\lambda$  412 nm in a spectrophotometric plate reader.

(iEMS Reader MF, Labsystems). Color generation is decreased as test compounds inhibit enzyme activity.  $IC_{50}$  values were calculated graphically at the concentration of compound that decreases enzyme activity by 50%, using a nonlinear regression (four-parameter logistic) method. Data are expressed as means  $\pm$  SEM of at least three different experiments in quadruplicate.

**Inhibition of hAChE and hBuChE:** The capacity of the new derivatives to inhibit cholinesterase activity was assessed using the method of Ellman et al.<sup>[41]</sup> Initial rate assays were performed at 37 °C with a Jasco V-530 double-beam spectrophotometer by following the rate of increase in absorbance at  $\lambda$  412 nm for 210 s. An AChE stock solution was prepared by dissolving human recombinant AChE (EC 3.1.1.7) lyophilized powder (Sigma, Italy) in 0.1 M phosphate buffer (pH 8.0) containing 0.1% Triton X-100. Stock solution of BuChE (EC 3.1.1.8) from human serum (Sigma, Italy) was prepared by dissolving the lyophilized powder in an aqueous solution of 0.1% gelatin. The final assay solution consisted of 0.1 M phosphate buffer (pH 8.0), with the addition of 340  $\mu$ M 5,5'-dithio-bis-(2-nitrobenzoic acid), 0.02 U mL<sup>-1</sup> human recombinant AChE, or BuChE from human serum, and 550  $\mu$ M substrate (acetylthiocholine iodide, or butyrylthiocholine iodide, respectively). Stock solutions of test compounds were prepared in methanol. Five different concentrations of inhibitor were selected in order to obtain enzyme inhibition between 20 and 80%. Assays were carried out with a blank containing all components except AChE or BuChE in order to account for any non-enzymatic reaction. Assay solutions (with and without inhibitor) were pre-incubated for 20 min at 37 °C before the addition of substrate. The reaction rates were compared, and the percent inhibition due to increasing inhibitor concentrations was calculated. Each concentration was analyzed in duplicate, and  $IC_{50}$  values were determined graphically from plots of log[concentration] versus percent inhibition (GraphPad Prism ver. 4.03, GraphPad Software Inc.).

**Oxygen radical absorbance capacity assay:** The radical scavenging capacity of the TFAHs was determined by the ORAC-FL method using fluorescein as a fluorescent probe.<sup>[42,43]</sup> (±)-6-Hydroxy-2,5,7,8-tetramethylchromane-2-carboxylic acid (trolox), fluorescein (FL) and 2,2'-azobis(aminopropane) dihydrochloride (AAPH) were purchased from Sigma-Aldrich. A Varioskan Flash plate reader with built-in injectors (Thermo Scientific) was used. The reaction was carried out at 37 °C in 75 mM phosphate buffer (pH 7.4), and the final reaction mixture volume was 200  $\mu$ L. The tested compounds and trolox standard were dissolved in DMSO to 10 mM and further diluted in 75 mM phosphate buffer (pH 7.4). The final concentrations were 0.1–1  $\mu$ M for the test compounds and 1–8  $\mu$ M for trolox. The blank was composed of 120  $\mu$ L FL, 60  $\mu$ L AAPH, and 20  $\mu$ L phosphate buffer (pH 7.4), and was added in each assay. In a black 96-well microplate (Nunc), antioxidant (20  $\mu$ L) and FL (120  $\mu$ L, final concentration: 70 nM) were incubated for 15 min at 37 °C. AAPH (60  $\mu$ L, final concentration: 40 mM) was then added rapidly using the built-in injector. The fluorescence was measured every minute for 60 min at  $\lambda_{ex}$  485 and  $\lambda_{em}$  535 nm. The microplate was automatically shaken prior to each reading. All reactions were carried out in triplicate and at least three different assays were performed for each sample. Antioxidant curves (fluorescence versus time) were first normalized to the curve of the blank (without antioxidant) and then the area under the fluorescence decay curve (AUC) was calculated as:  $AUC = 1 + \sum(f_i/f_0)$ , for which  $f_0$  is the initial fluorescence reading at 0 min and  $f_i$  is the fluorescence value at time  $i$ .

The net AUC corresponding to a sample was calculated as follows: Net AUC = AUC<sub>antioxidant</sub> – AUC<sub>blank</sub>. Regression equations were calculated by plotting the net AUC against the antioxidant concentra-

tion. The ORAC value was obtained by dividing the slope of the latter curve between the slope of the trolox curve obtained in the same assay. Final ORAC values were expressed as  $\mu$ mol trolox per  $\mu$ mol TFAH; data are expressed as means  $\pm$  SD.

**Kinetic inhibition studies:** To estimate the mode of inhibition of TFAH 10h, Lineweaver–Burk double-reciprocal plots were constructed at relatively low substrate concentrations (0.11–0.56  $\mu$ M). The plots were assessed by a weighted least-square analysis that assumed the variance of  $v$  to be a constant percentage of  $v$  for the entire data set. Data analysis was performed with GraphPad Prism ver. 4.03 software (GraphPad Software Inc.). Calculation of the inhibition constant ( $K_i$ ) value was carried out by re-plotting slopes of lines from the Lineweaver–Burk plot versus the inhibitor concentration, and  $K_i$  was determined as the intersect on the negative x-axis.  $K_i$  (dissociation constant for the enzyme–substrate–inhibitor complex) value was determined by plotting the apparent  $1/v_{max}$  versus inhibitor concentration.<sup>[68]</sup>

**Inhibition of A $\beta_{1-42}$  self-aggregation:** 1,1,1,3,3,3-Hexafluoro-2-propanol (HFIP) pre-treated A $\beta_{1-42}$  samples (Bachem AG, Switzerland) were re-solubilized with a mixture of CH<sub>3</sub>CN/Na<sub>2</sub>CO<sub>3</sub>/NaOH (48.4:48.4:3.2) to generate a stable stock solution ([A $\beta_{1-42}$ ] = 500  $\mu$ M).<sup>[44]</sup> Experiments were performed by incubating the peptide in 10 mM phosphate buffer (pH 8.0) containing 10 mM NaCl at 30 °C for 24 h (final A $\beta$  concentration: 50  $\mu$ M) with and without inhibitor (50  $\mu$ M). The inhibitor was dissolved in methanol and diluted in the assay buffer. Blanks containing inhibitor and ThT were also prepared and evaluated to account for quenching and fluorescence properties. To quantify amyloid fibril formation, the ThT fluorescence method was used.<sup>[69,70]</sup> After incubation, samples were diluted to a final volume of 2.0 mL with 50  $\mu$ M glycine-NaOH buffer (pH 8.5) containing 1.5  $\mu$ M ThT. A time scan (300 s) of fluorescence intensity was carried out ( $\lambda_{ex}$  446,  $\lambda_{em}$  490 nm), and values at plateau were averaged after subtracting the background fluorescence of 1.5  $\mu$ M ThT solution. The fluorescence intensities were compared and the percent inhibition was calculated.

### Docking simulations

The geometry of the ligands was optimized using the ab initio quantum chemistry program Gaussian 09 and the B3LYP/3-21G\* basis set. A set of atom-centered RHF 6-31G\* charges was then obtained by using the RESP methodology.<sup>[71]</sup> The X-ray crystal structure of *E. electricus* acetylcholinesterase was retrieved from the Protein Data Bank (PDB ID: 1C2B)<sup>[72]</sup> as target protein. Missing atoms were reconstructed with SwissPDB Viewer 4.1.0.<sup>[73]</sup> The docking experiments were carried out using the Lamarckian genetic algorithm implemented in AutoDock 4.2.<sup>[74]</sup> A box encompassing both the CAS and PAS sites was defined for the exploration of possible binding modes. A volume for exploration was defined within a 3D cubic grid (60  $\times$  74  $\times$  60 Å<sup>3</sup>) at a resolution of 0.3 Å and centered on the gorge that encloses the regions that are known to make up the inhibitor binding pockets and modes. Affinity grid files were generated using the auxiliary program AutoGrid. At each grid point, the receptor's atomic affinity potentials for carbon, oxygen, nitrogen, chlorine, and hydrogen atoms present in the ligand were pre-calculated for rapid intra- and intermolecular energy evaluation of the docking solution. Different conformers of the ligands were docked by randomly changing the torsion angles and overall orientation of the molecule. The receptor residues Trp286, Tyr124, Tyr337, Tyr72, Asp74, Thr75, Trp86, and Tyr341 were selected to remain flexible during docking simulation with the AutoTors module. The program searched until a maximum of 100 conforma-

tions, and the procedure was repeated 100 times (runs). After docking, the 100 solutions were clustered in groups with RMSDs < 1.5 Å. The clusters were ranked by the lowest-energy representative of each cluster. For all other parameters, the default values were used with AutoDock Tools. Given the lack of a crystal structure for eqBuChE, a homology model was used to rationalize experimental data. To this end, the automated homology-modeling SWISS-MODEL program was used to perform the modeling of the 3D structure.<sup>[73]</sup> The 3D structure of eqBuChE was created (UniProt Q9N1N9, modeled residue range: 32–562) based on the crystal structure of hBuChE (PDB ID: 2PM8).<sup>[75]</sup> Docking calculations were performed by following the same protocol described above for EeAChE. We also performed docking simulations with the crystal structure of hBuChE in complex with tacrine as protein target (PDB ID: 4BDS).<sup>[46]</sup> The results revealed that the tacrine moiety of TFAH **10b** occupies the same position as that observed in the original complex with tacrine (RMSD = 0.5 Å). Moreover, the ligand binding pose is equivalent to that found for the docking study with the modeled 3D structure of eqBuChE. The same docking protocol was applied for the binding studies of TFAHs **10e** and **10h** with the structure of human acetyl- (PDB ID: 4EY7)<sup>[45]</sup> and butyrylcholinesterase (PDB ID: 4BDS)<sup>[46]</sup> as target proteins. Analogously, the docking experiments were carried out using the Lamarckian genetic algorithm implemented in AutoDock 4.2.

The docking method with the inclusion of seven structural water molecules was performed with GOLD ver. 5.2 according to the method published by Darras et al.<sup>[49,76]</sup> In preliminary docking runs the tacrine showed hydrogen bond interactions with the catalytic residue Ser203. Thus, a mild hydrogen bond constraint was placed on the hydroxy oxygen atom to obtain an optimized binding pose. The top-scored pose is shown in Figure 5. Distances were measured between heavy atoms or between the heavy atom and the geometric center of the His ring in PyMOL.<sup>[50]</sup>

### Ex vivo brain penetration study

To test brain permeability, the compound **10a** was subjected to an ex vivo determination of its AChE inhibitory activity, as previously described.<sup>[64,77]</sup> Briefly, the compound was administered intraperitoneally (i.p.) to young adult Wistar rats (2 months of age) at either 10 or 50  $\mu\text{mol kg}^{-1}$ . Experiments were performed in accordance with the Italian and European Community law for the use of experimental animals and were approved by a local bioethical committee. Animals were killed by decapitation at 2 h after injection; brain tissue was immediately dissected, and cortices from both hemispheres were collected. Tissues were homogenized in ice-cold 50 mM Tris-HCl buffer at pH 7.4, and Triton X-100 was added to a final concentration of 0.5% (all chemicals from Sigma-Aldrich). Homogenates were used to assay AChE activity according to the standard colorimetric method,<sup>[41]</sup> and to measure the total protein content for normalization.<sup>[78]</sup> AChE inhibition was not observed under the conditions used here.

*In vitro* blood–brain barrier permeation assay (PAMPA-BBB): Prediction of brain penetration was evaluated by using a parallel artificial membrane permeation assay (PAMPA-BBB), in a similar manner as previously described.<sup>[16,62,63]</sup> Pipetting was performed with a semiautomatic pipetter (CyBi-SELMA), and UV reading with a microplate spectrophotometer (Multiskan Spectrum, Thermo Electron Co.). Commercial drugs, PBS (pH 7.4), and dodecane were purchased from Sigma, Aldrich, Acros, and Fluka. Millex filter units (PVDF membrane,  $\varnothing$  = 25 mm, pore size = 0.45  $\mu\text{m}$ ) were acquired from Millipore. Porcine brain lipid (PBL) was obtained from Avanti Polar

Lipids. The donor microplate was a 96-well filter plate (PVDF membrane, pore size = 0.45  $\mu\text{m}$ ), and the acceptor microplate was an indented 96-well plate, both from Millipore. The acceptor 96-well microplate was filled with 200  $\mu\text{L}$  PBS/EtOH (70:30 v/v), and the filter surface of the donor microplate was impregnated with 4  $\mu\text{L}$  PBL in dodecane (20  $\text{mg mL}^{-1}$ ). Compounds were dissolved in PBS/EtOH (70:30 v/v) at 100  $\mu\text{g mL}^{-1}$ , filtered through a Millex filter, and then added to the donor wells (200  $\mu\text{L}$ ). The donor filter plate was carefully put on the acceptor plate to form a sandwich, which was left undisturbed for 120 min at 25 °C. After incubation, the donor plate was carefully removed, and the concentration of compounds in the acceptor wells was determined by UV/Vis spectroscopy. Every sample was analyzed at five wavelengths, in four wells and in at least three independent runs; results are given as the mean  $\pm$  standard deviation. In each experiment, 11 quality control standards of known BBB permeability were included to validate the analysis set.

### Glossary

AAPH = 2,2'-azobis(amidinopropane) dihydrochloride; A $\beta$  =  $\beta$ -amyloid; ACh = acetylcholine; AChE = acetylcholinesterase; AChEIs = acetylcholinesterase inhibitors; AD = Alzheimer's disease; ADMET = absorption, distribution, metabolism, excretion, toxicity; ATCh = acetylthiocholine iodide; BBB = blood–brain barrier; BuChE = butyrylcholinesterase; BTCh = butyrylthiocholine iodide; CAS = catalytic anionic site; ChEs = cholinesterases; DMSO = dimethyl sulfoxide; DTNB = 5,5'-dithiobis-2-nitrobenzoic acid; EDTA = 2,2',2''',2'''-(ethane-1,2-diyl)dinitrilo)tetraacetic acid; EeAChE = *Electrophorus electricus* acetylcholinesterase; eqBuChE = equine butyrylcholinesterase; EMEM = Eagle's minimum essential medium; FA = ferulic acid; FBS = fetal bovine serum; FDA = US Food and Drug Administration; FL = fluorescein; hAChE = human recombinant acetylcholinesterase; hAChEIs = human recombinant acetylcholinesterase inhibitors; hBuChE = human serum butyrylcholinesterase; hChEs = human cholinesterases; HepG2 = human liver hepatocellular carcinoma cell line; HFIP = 1,1,1,3,3,3-hexafluoro-2-propanol; MDTLs = multitarget-directed ligands; 7-MEOTA = 9-amino-7-methoxy-1,2,3,4-tetrahydroacridine; MTT = 3-(4,5-dimethylthiazol-2-yl)-2,5-diphenyltetrazolium bromide; NFT = neurofibrillary tangles; O/R = oligomycin A/rotenone; ORAC-FL = oxygen radical absorbance capacity-fluorescein; PAMPA = parallel artificial membrane permeability assay; PAS = peripheral anionic site; PBL = porcine brain lipid; PC12 = rat pheochromocytoma cell line; ROS = reactive oxygen species; SH-SY5Y = human dopaminergic neuroblastoma cell line; TFAHs = tacrine-ferulic acid hybrids; ThT = thioflavin T; U-4CR = Ugi four-component reaction.

### Acknowledgements

The authors thank the Regional Council of Franche-Comté (France) for financial support and for the award of a PhD grant to M. Benckekroun. We also thank Ms. Marie-Jeanne Henriot (PHV Pharma, Domblans, France) for technical support in HPLC measurements. Appreciation is expressed to Professor C. A. Sotriffer (University of Würzburg, Germany) for helpful discussions with S. Wehle. We gratefully acknowledge the German Academic National Foundation (Studienstiftung des deutschen Volkes) for awarding a PhD scholarship to S. Wehle. M. I. Rodríguez-Franco acknowledges financial support from the Spanish Ministry of Economy and Competitiveness (SAF2012-31035), CSIC (PIE-



201280E074), and the Fundación de Investigación Médica Mutua Madrileña Automovilística (AP103952012).

**Keywords:** Alzheimer's disease • antioxidants • cholinesterases • inhibitors • multicomponent reactions • neuroprotection

- [1] P. Davies, A. J. Maloney, *Lancet* **1976**, 2, 1403.
- [2] R. T. Bartus, R. L. Dean III, B. Beer, A. S. Lippa, *Science* **1982**, 217, 408–414.
- [3] A. Cavalli, M. L. Bolognesi, A. Minarini, M. Rosini, V. Tumiatti, M. Recanatini, C. Melchiorre, *J. Med. Chem.* **2008**, 51, 347–372.
- [4] I. Tomassoli, L. Ismaili, M. Pudlo, C. de Los Ríos, E. Soriano, I. Colmena, L. Gandía, L. Rivas, A. Samadi, J. Marco-Contelles, B. Refouvet, *Eur. J. Med. Chem.* **2011**, 46, 1–10.
- [5] A. Andreani, S. Burnelli, M. Granaola, M. Guardigli, A. Leoni, A. Locatelli, R. Morigi, M. Rambaldi, M. Rizzoli, L. Varoli, A. Roda, *Eur. J. Med. Chem.* **2008**, 43, 657–661.
- [6] D. Silva, M. Chioua, A. Samadi, P. Agostinho, P. Garção, R. Lajarin-Cuesta, C. de Los Ríos, I. Iriepa, I. Moraleda, L. Gonzalez-Lafuente, E. Mendes, C. Perez, M. I. Rodriguez-Franco, J. Marco-Contelles, M. C. Carmo, *ACS Chem. Neurosci.* **2013**, 4, 547–565.
- [7] H. Soreq, S. Seidman, *Nat. Rev. Neurosci.* **2001**, 2, 294–302.
- [8] M. Bartolini, C. Bertucci, V. Cavrini, V. Andrisano, *Biochem. Pharmacol.* **2003**, 65, 407–416.
- [9] A. Tasker, E. K. Perry, C. G. Ballard, *Expert Rev. Neurother.* **2005**, 5, 101–106.
- [10] Y. Furukawa-Hibi, T. Alkam, A. Nitta, A. Matsuyama, H. Mizoguchi, K. Suzuki, S. Moussaoui, Q.-S. Yu, N. H. Greig, T. Nagai, K. Yamada, *Behav. Brain Res.* **2011**, 225, 222–229.
- [11] L.-E. Cassagnes, V. Hervé, F. Nepveu, C. Hureau, P. Faller, F. Collin, *Angew. Chem. Int. Ed.* **2013**, 52, 11110–11113; *Angew. Chem.* **2013**, 125, 11316–11319.
- [12] Y. Christen, *Am. J. Clin. Nutr.* **2000**, 71, 621S–629S.
- [13] A. Contestabile, *Behav. Brain Res.* **2011**, 221, 334–340.
- [14] M. J. Knapp, D. S. Knopman, P. R. Solomon, W. W. Pendlebury, C. S. Davis, S. I. Gracon, *JAMA J. Am. Med. Assoc.* **1994**, 271, 985–991.
- [15] P. B. Watkins, H. J. Zimmerman, M. J. Knapp, S. I. Gracon, K. W. Lewis, *JAMA J. Am. Med. Assoc.* **1994**, 271, 992–998.
- [16] M. I. Fernández-Bachiller, C. Pérez, L. Monjas, J. Rademann, M. I. Rodríguez-Franco, *J. Med. Chem.* **2012**, 55, 1303–1317.
- [17] J. Patocka, D. Jun, K. Kuca, *Curr. Drug Metab.* **2008**, 9, 332–335.
- [18] J. Patocka, *Sb. Ved. Pr. Lek. Fak. Univ. Karlovy Hradec Kralove* **1986**, 102, 123–140.
- [19] J. L. Marx, *Science* **1987**, 238, 1041–1042.
- [20] D. J. Ames, P. S. Bhathal, B. M. Davies, J. R. Fraser, *Lancet* **1988**, 1, 887.
- [21] A. Romero, R. Cacabelos, M. J. Oset-Gasque, A. Samadi, J. Marco-Contelles, *Bioorg. Med. Chem. Lett.* **2013**, 23, 1916–1922.
- [22] Y. Chen, J. Sun, L. Fang, M. Liu, S. Peng, H. Liao, J. Lehmann, Y. Zhang, *J. Med. Chem.* **2012**, 55, 4309–4321.
- [23] X. Chao, X. He, Y. Yang, X. Zhou, M. Jin, S. Liu, Z. Cheng, P. Liu, Y. Wang, J. Yu, Y. Tan, Y. Huang, J. Qin, S. Rapposelli, R. Pi, *Bioorg. Med. Chem. Lett.* **2012**, 22, 6498–6502.
- [24] L. Fang, B. Kraus, J. Lehmann, J. Heilmann, Y. Zhang, M. Decker, *Bioorg. Med. Chem. Lett.* **2008**, 18, 2905–2909.
- [25] R. Pi, X. Mao, X. Chao, Z. Cheng, M. Liu, X. Duan, M. Ye, X. Chen, Z. Mei, P. Liu, W. Li, Y. Han, *PLoS One* **2012**, 7, e31921.
- [26] J. E. Biggs-Houck, A. Younai, J. T. Shaw, *Curr. Opin. Chem. Biol.* **2010**, 14, 371–382.
- [27] A. Basiri, V. Murugaiyah, H. Osman, R. S. Kumar, Y. Kia, K. B. Awang, M. A. Ali, *Eur. J. Med. Chem.* **2013**, 67, 221–229.
- [28] O. Di Pietro, E. Viayna, E. Vicente-García, M. Bartolini, R. Ramón, J. Juárez-Jiménez, M. V. Clos, B. Pérez, V. Andrisano, F. J. Luque, R. Lavilla, D. Muñoz-Torrero, *Eur. J. Med. Chem.* **2014**, 73, 141–152.
- [29] O. Di Pietro, F. J. Pérez-Areales, J. Juárez-Jiménez, A. Espargaró, M. V. Clos, B. Pérez, R. Lavilla, R. Sabaté, F. J. Luque, D. Muñoz-Torrero, *Eur. J. Med. Chem.* **2014**, 84, 107–117.
- [30] A. Dömling, W. Wang, K. Wang, *Chem. Rev.* **2012**, 112, 3083–3135.
- [31] T. J. Dickerson, A. E. Beuscher, C. J. Rogers, M. S. Hixon, N. Yamamoto, Y. Xu, A. J. Olson, K. D. Janda, *Biochemistry* **2005**, 44, 14845–14853.
- [32] N. C. Inestrosa, A. Alvarez, C. A. Pérez, R. D. Moreno, M. Vicente, C. Linker, O. I. Casanueva, C. Soto, J. Garrido, *Neuron* **1996**, 16, 881–891.
- [33] P. R. Carlier, E. S.-H. Chow, Y. Han, J. Liu, J. E. Yazal, Y.-P. Pang, *J. Med. Chem.* **1999**, 42, 4225–4231.
- [34] J. Bielavský, *Collect. Czech. Chem. Commun.* **1977**, 42, 2802–2808.
- [35] M. R. Del Giudice, A. Borioni, C. Mustazza, F. Gatta, A. Meneguz, M. T. Volpe, *Farmaco* **1996**, 51, 693–698.
- [36] K. Pérez-Labrada, I. Brouard, I. Méndez, D. G. Rivera, *J. Org. Chem.* **2012**, 77, 4660–4670.
- [37] M. Esquivias-Pérez, E. Maalej, A. Romero, F. Chabchoub, A. Samadi, J. Marco-Contelles, M. J. Oset-Gasque, *Chem. Res. Toxicol.* **2013**, 26, 986–992.
- [38] F. Denizot, R. Lang, *J. Immunol. Methods* **1986**, 89, 271–277.
- [39] C. Shi, L. Zhao, B. Zhu, Q. Li, D. T. Yew, Z. Yao, J. Xu, *Chem.-Biol. Interact.* **2009**, 181, 115–123.
- [40] G. C. González-Muñoz, M. P. Arce, B. López, C. Pérez, A. Romero, L. del Barrio, M. D. Martín-de-Saavedra, J. Egea, R. León, M. Villarroya, M. G. Lopez, A. G. Garcia, S. Conde, M. I. Rodríguez-Franco, *Eur. J. Med. Chem.* **2011**, 46, 2224–2235.
- [41] G. L. Ellman, K. D. Courtney, V. Andres, Jr., R. M. Featherstone, *Biochem. Pharmacol.* **1961**, 7, 88–95.
- [42] B. Ou, M. Hampsch-Woodill, R. L. Prior, *J. Agric. Food Chem.* **2001**, 49, 4619–4626.
- [43] A. Dávalos, C. Gómez-Cordovés, B. Bartolomé, *J. Agric. Food Chem.* **2004**, 52, 48–54.
- [44] M. Bartolini, C. Bertucci, M. L. Bolognesi, A. Cavalli, C. Melchiorre, V. Andrisano, *ChemBioChem* **2007**, 8, 2152–2161.
- [45] J. Cheung, M. J. Rudolph, F. Burshteyn, M. S. Cassidy, E. N. Gary, J. Love, M. C. Franklin, J. J. Height, *J. Med. Chem.* **2012**, 55, 10282–10286.
- [46] F. Nachon, E. Carletti, C. Ronco, M. Trovaslet, Y. Nicolet, L. Jean, P.-Y. Renard, *Biochem. J.* **2013**, 453, 393–399.
- [47] J. Korabecny, K. Musilek, O. Holas, J. Binder, F. Zemek, J. Marek, M. Pohanka, V. Opletalova, V. Dohnal, K. Kuca, *Bioorg. Med. Chem. Lett.* **2010**, 20, 6093–6095.
- [48] I. Bolea, J. Juárez-Jiménez, C. de Los Ríos, M. Chioua, R. Pouplana, F. J. Luque, M. Unzeta, J. Marco-Contelles, A. Samadi, *J. Med. Chem.* **2011**, 54, 8251–8270.
- [49] F. H. Darras, S. Wehle, G. Huang, C. A. Sotriffer, M. Decker, *Bioorg. Med. Chem.* **2014**, 22, 4867–4881.
- [50] The PyMOL Molecular Graphics System, Version 1.6.0.0, Schrödinger LLC, New York, NY (USA), **2013**.
- [51] ADMET Predictor ver. 6.5, Simulations Plus Inc., Lancaster, CA (USA), **2013**.
- [52] ACD/Percepta ver. 14.0.0, Advanced Chemistry Development Inc., Toronto, ON (Canada), **2013**.
- [53] Schrödinger Suite 2013-3: QuickProp, ver. 3.8, Schrödinger LLC, New York, NY (USA), **2013**.
- [54] I. Moriguchi, S. Hirono, Q. Liu, I. Nakagome, Y. Matsushita, *Chem. Pharm. Bull.* **1992**, 40, 127–130.
- [55] C. A. Lipinski, F. Lombardo, B. W. Dominy, P. J. Feeney, *Adv. Drug Delivery Rev.* **2001**, 46, 3–26.
- [56] F. Atkinson, S. Cole, C. Green, H. van de Waterbeemd, *Curr. Med. Chem. Cent. Nerv. Syst. Agents* **2002**, 2, 229–240.
- [57] J. Kelder, P. D. Grootenhuys, D. M. Bayada, L. P. Delbressine, J. P. Ploemen, *Pharm. Res.* **1999**, 16, 1514–1519.
- [58] T. T. Wager, R. Y. Chandrasekaran, X. Hou, M. D. Troutman, P. R. Verhoest, A. Villalobos, Y. Will, *ACS Chem. Neurosci.* **2010**, 1, 420–434.
- [59] M. P. Gleeson, *J. Med. Chem.* **2008**, 51, 817–834.
- [60] P. A. Nielsen, O. Andersson, S. H. Hansen, K. B. Simonsen, G. Andersson, *Drug Discovery Today* **2011**, 16, 472–475.
- [61] L. Di, E. H. Kerns, K. Fan, O. J. McConnell, G. T. Carter, *Eur. J. Med. Chem.* **2003**, 38, 223–232.
- [62] M. I. Rodríguez-Franco, M. I. Fernández-Bachiller, C. Pérez, B. Hernández-Ledesma, B. Bartolomé, *J. Med. Chem.* **2006**, 49, 459–462.
- [63] B. López-Iglesias, C. Pérez, J. A. Morales-García, S. Alonso-Gil, A. Pérez-Castillo, A. Romero, M. G. López, M. Villarroya, S. Conde, M. I. Rodríguez-Franco, *J. Med. Chem.* **2014**, 57, 3773–3785.

- [64] M. Rosini, E. Simoni, M. Bartolini, E. Soriano, J. Marco-Contelles, V. Andrisano, B. Monti, M. Windisch, B. Hutter-Paier, D. W. McClymont, I. R. Mellor, M. L. Bolognesi, *ChemMedChem* **2013**, *8*, 1276–1281.
- [65] T. Arendt, M. K. Brückner, M. Lange, V. Bigl, *Neurochem. Int.* **1992**, *21*, 381–396.
- [66] S. Darvesh, D. A. Hopkins, C. Geula, *Nat. Rev. Neurosci.* **2003**, *4*, 131–138.
- [67] N. H. Greig, T. Utsuki, D. K. Ingram, Y. Wang, G. Pepeu, C. Scali, Q.-S. Yu, J. Mamczarz, H. W. Holloway, T. Giordano, D. M. Chen, K. Furukawa, K. Sambamurti, A. Brossi, D. K. Lahiri, *Proc. Natl. Acad. Sci. USA* **2005**, *102*, 17213–17218.
- [68] R. B. Silverman, *The Organic Chemistry of Enzyme-Catalyzed Reactions*, Academic Press, San Diego, **2000**.
- [69] H. Naiki, K. Higuchi, M. Hosokawa, T. Takeda, *Anal. Biochem.* **1989**, *177*, 244–249.
- [70] H. Levine III, *Protein Sci.* **1993**, *2*, 404–410.
- [71] A. J. S. Knox, M. J. Meegan, D. G. Lloyd, *Curr. Top. Med. Chem.* **2006**, *6*, 217–243.
- [72] Y. Bourne, J. Grassi, P. E. Bougis, P. Marchot, *J. Biol. Chem.* **1999**, *274*, 30370–30376.
- [73] SwissPDB Viewer ver. 4.1.0, GlaxoSmithKline R&D, Switzerland, **2012**.
- [74] G. M. Morris, R. Huey, W. Lindstrom, M. F. Sanner, R. K. Belew, D. S. Goodsell, A. J. Olson, *J. Comput. Chem.* **2009**, *30*, 2785–2791.
- [75] M. N. Ngamelue, K. Homma, O. Lockridge, O. A. Asojo, *Acta Crystallogr. Sect. F* **2007**, *63*, 723–727.
- [76] GOLD Suite 5.2, CCDC Software, www.ccdc.cam.ac.uk, **2013**.
- [77] E. Nepovimova, E. Uliassi, J. Korabecny, L. E. Peña-Altamira, S. Samez, A. Pesaresi, G. E. Garcia, M. Bartolini, V. Andrisano, C. Bergamini, R. Fato, D. Lamba, M. Roberti, K. Kuca, B. Monti, M. L. Bolognesi, *J. Med. Chem.* **2014**, *57*, 8576–8589.
- [78] O. H. Lowry, N. J. Rosebrough, A. L. Farr, R. J. Randall, *J. Biol. Chem.* **1951**, *193*, 265–275.

Received: September 22, 2014

Published online on ■ ■ ■, 0000



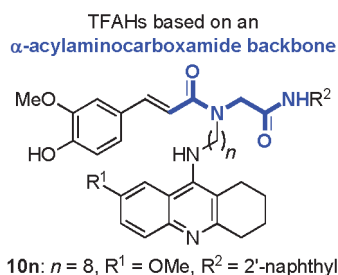
## FULL PAPERS

M. Benchekroun, M. Bartolini, J. Egea,  
A. Romero, E. Soriano, M. Pudlo, V. Luzet,  
V. Andrisano, M.-L. Jimeno, M. G. López,  
S. Wehle, T. Gharbi, B. Refouvelet,  
L. de Andrés, C. Herrera-Arozamena,  
B. Monti, M. L. Bolognesi,  
M. I. Rodríguez-Franco, M. Decker,  
J. Marco-Contelles,\* L. Ismaili\*

■■■ – ■■■



**Novel Tacrine-Grafted Ugi Adducts as  
Multipotent Anti-Alzheimer Drugs: A  
Synthetic Renewal in Tacrine–Ferulic  
Acid Hybrids**



**Multicomponent reaction** for a multifactorial disease: new multipotent tacrine–ferulic acid hybrids (TFAHs) were synthesized by the Ugi four-component reaction and evaluated in vitro for the treatment of Alzheimer’s disease. Among them, TFAH **10n** was found to selectively inhibit human butyrylcholinesterase. It also demonstrated good profiles in terms of toxicity, neuroprotection, antioxidant, and blood–brain barrier penetration.